EFFECT OF RANDOM STRUCTURAL VARIATIONS ON THE OPTICAL PROPERTIES OF HONEYCOMB PHOTONIC CRYSTALS

A Thesis Submitted to
the Graduate School of
İzmir Institute of Technology
in Partial Fulfillment of the Requirements for the Degree of

MASTER OF SCIENCE

in Physics

by
Yiğit TUNÇTÜRK

December 2021
İZMİR

ACKNOWLEDGMENTS

I would like to thank my supervisor, Assoc. Prof. Dr. H. Sami SÖZÜER who has given me a chance to get my Masters degree. Without his guidance and belief in me, this work would not be possible.

I would also like to thank my group friend Zebih ÇETİN who is the most patient man I have ever met.

I also want to thank my friends Hacer ÇINAR, Gürcan COŞGEL, Emre OKÇU, Sinem DUMAN, Ersin YILDIZ, Koray SEVİM and Ayşenur BİRİNCİ for their endless support and friendship.

Finally, I thank my mother Commander Birhan TUNÇTÜRK TRN (Ret.) who has three bachleor degrees and always makes fun of me and my friends.

ABSTRACT

EFFECT OF RANDOM STRUCTURAL VARIATIONS ON THE OPTICAL PROPERTIES OF HONEYCOMB PHOTONIC CRYSTALS

Periodic dielectric structures called photonic crystals(PhCs) are being used in various sensors and devices. Since PhCs are designed to operate within certain frequency ranges, accuracy in structure becomes important. During the manufacturing process, random errors in geometry can be encountered. Two types of errors come to the forefront, surface roughness and positional randomness. Once the periodic structure becomes imperfect due to random errors, calculations for the desired frequency ranges must be performed using supercells. In this thesis, effect of surface roughness and positional randomness on photonic density of states are investigated for both TM and TE modes in two-dimensional honeycomb photonic crystals.

ÖZET

RASTGELE YAPISAL VARYASYONLARIN BAL PETEĞİ FOTONİK KRİSTALLERİN OPTİK ÖZELLİKLERİ ÜZERİNE ETKİSİ

Fotonik kristaller adı verilen periyodik dielektirik yapılar çeşitli sensör ve cihazlarda kullanılmaktadırlar. Fotonik kristaller belirli frekans aralıklarında çalışacak ş ekilde tasarlandıklarında, yapılarındaki doğruluk önemli hale gelir. İmalat işlemi esnasında geometride rastgele hatalarla karşılaşılabilir. Yüzey pürüzlülüğü ve konumsal rastgelelik olmak üzere iki tür hata ön plana çıkmaktadır. Rastgele hatalar nedeniyle yapı tamamen asimetrik bir hale geldiğinde, istenen frekans aralıkları için hesaplamalar süperhücrelerde yapılmalıdır. Bu tezde, iki boyutlu balpeteği fotonik kristalinde hem TM hem de TE modları için yüzey pürüzlülüğü ve konumsal rastgeleliğin fotonik durum yoğunluğu üzerindeki etkisi araştırılmıştır.

TABLE OF CONTENTS

LIST OF FIGURES

Figure **Page**

Figure **Page**

Figure **Page**

CHAPTER 1

INTRODUCTION

Only ten years ago, devices that can be called ”Sci-Fi Gadgets” became real things thanks to dedicated scientists, engineers and massive investments of technology companies and visionary multibillionaires. Some of these devices can gather information and share instantly. For an example, smart watches which have EKG(electrocardiogram) and pulse oximetry features. Numerous kinds of sensors in biotechnology (Chu et al. (2020); Yoo et al. (2021)), machine vision (Liu et al. (2021)) and arms industry (Cullen et al. (2011)) areas are integrated into circuits and an era has changed. The semi-conductors of light called photonic crystals(PhCs) cleared the way for many these sensors when the topic is related to light. However, PhCs were being used by nature way before people knew about them (Vigneron and Simonis (2012)).

PhCs are designed to operate in certain frequencies of light. The determinants of them are mostly geometry and characteristics of the materials used. Easiest way to understand behaviour of these frequencies is visualization them against Bloch vectors which called photonic bandgap(PBG) diagrams.It all started with the paper of Yablonovitch (Yablonovitch (1987)). The idea behind the PBG was preventing spontaneous emissions using periodic dielectric structures and understanding how it works. Along with that, John (John (1987)) studied strongly localization of EM waves in periodic dielectric materials. When intentionally constraining propagation of light becomes a real thing, interest in PhCs skyrocketed.

While PhCs are used in such crucial areas intensely we can not ignore the effect of randomly occurred structural erros. Even in nature, these errors result in interesting consequences which are showed by the work of Mouchet et al. (2020). When survivability depends on camouflage, mother nature is the best designer of the PhCs. Nature aside, these errors can be encountered during fabrication process. These errors are typically variations in the diameters or locations of holes, spheres, rods or thickness of slabs etc. One can easily find good examples as TEM(Transmission Electron Microscopy) and SEM(Scanning Electron Microscopy) images in the papers of Asif et al. (2011) Zhang

et al. (2020) and Kim et al. (2012) for different shapes of PhCs.

In any case, they directly affect the PBGs substantially. Feng et al. (2006) reported the effect of rotational and surface erros on focusing two dimensional photonic crystal flat lenses. Errors in a square lattice of dielectric rods Badreldin and Khalil (2006) showed these kinds of errors do actually cause trouble. Effect of positional disorder in square and triangular structures for both TM(Transverse Magnetic) and TE(Transverse Electric) modes are shown by work of Meisels and Kuchar (2007). In one dimensional cases, Sözüer and Sevim (2005) and Kong et al. (2011) are good examples.

Among other prominent structures, two dimensional dielectric rods in a honeycomb lattice is a fundamental case. In this thesis, what we have studied is the endurance limits of complete photonic band-gaps(CPBG) and change in transmission against random structural variations in two dimensional honeycomb PhCs of dielectric rods in air. These variations are in the surfaces and locations of rods basically.

Calculating frequencies for all $k - points$ on the supercell is impossible due to limited resources. As an effective method we used a reasonable number of random $k - points$. At that point, band structures become incoherent so we preferred to work on density of states(DOS). Since we work in two-dimensional space, electromagnetic modes can be separated into transverse-magnetic and transverse-electric modes. Investigating DOS and transmission of both modes individually is an advantage to understand what really happens to the CPBG.

CHAPTER 2

METHODOLOGY

In this work we used two open-source software packages, MPB(MIT Photonic Bands) (Johnson and Joannopoulos (2001)) and MEEP(MIT Electromagnetic Equation Propagation) (Oskooi et al. (2010)) . Band frequencies were calculated by MPB using the method called plane wave expansion method. For transmission calculations, MEEP uses the Finite Difference Time Domain (FDTD) method.

2.1. Plane Wave Expansion With H Method

Starting with microscopic Maxwell's equations,

$$\nabla \cdot \mathbf{B} = 0 \tag{2.1}$$

$$\nabla \cdot \mathbf{E} = \rho/\varepsilon_0 \tag{2.2}$$

$$\nabla \times \mathbf{B} = \mu_0 \mathbf{J} + \varepsilon_0 \frac{\partial \mathbf{E}}{\partial t} \tag{2.3}$$

$$\nabla \times \mathbf{E} = -\frac{\partial \mathbf{B}}{\partial t} \tag{2.4}$$

Here ρ is the charge density, ε_0 is the permittivity of free space, $\mathbf{J}$ is the current density and μ_0 is the permeability of free space. Additionally, we need to define the electric displacement $\mathbf{D}$, and magnetic field strength $\mathbf{H}$ as,

$$\mathbf{D} \equiv \varepsilon_0 \mathbf{E} + \mathbf{P} = \mathbf{D}(\mathbf{E}) \tag{2.5}$$

$$\mathbf{H} \equiv \mu_0 \mathbf{B} - \mathbf{M} = \mathbf{H}(\mathbf{B}) \tag{2.6}$$

where $\mathbf{P}$ is the electric polarization, and $\mathbf{M}$ is the magnetization. Then the microscopic

equations become macroscopic with these definitions.

$$\nabla \cdot \mathbf{B} = 0 \tag{2.7}$$

$$\nabla \cdot \mathbf{D} = \rho_f \tag{2.8}$$

$$\nabla \times \mathbf{H} = \mathbf{J}_f + \frac{\partial \mathbf{D}}{\partial t} \tag{2.9}$$

$$\nabla \times \mathbf{E} = -\frac{\partial \mathbf{B}}{\partial t} \tag{2.10}$$

Assuming light propagates through the linear, non-dispersive, non-lossy crystal while no free charges and currents around so we can set $\rho_f = 0$, $\mathbf{J}_f = 0$, $\mathbf{D} = \varepsilon_0 \varepsilon(\mathbf{r})\mathbf{E}$ and $\mathbf{B} = \mu_0 \mu(\mathbf{r})\mathbf{H}$. Also, $\varepsilon(\mathbf{r})$ and $\mu(\mathbf{r})$ are allowed to vary in space.
Now, the equations 2.9 and 2.10 need to be rewritten using the assumptions above,

$$\nabla \times \mathbf{H} = \frac{\partial \mathbf{D}}{\partial t} = \varepsilon_0 \varepsilon(\mathbf{r}) \frac{\partial \mathbf{E}}{\partial t} \tag{2.11}$$

$$\nabla \times \mathbf{E} = -\frac{\partial \mathbf{B}}{\partial t} = -\mu_0 \mu(\mathbf{r}) \frac{\partial \mathbf{H}}{\partial t} \tag{2.12}$$

after dividing both sides of the equation 2.11 by $\varepsilon(\mathbf{r})$ and taking curl we have,

$$\nabla \times \left(\frac{1}{\varepsilon(\mathbf{r})} (\nabla \times \mathbf{H}) \right) = \varepsilon_0 \frac{\partial (\nabla \times \mathbf{E})}{\partial t} \tag{2.13}$$

using the equation 2.12 for the equation 2.13

$$\nabla \times \left(\frac{1}{\varepsilon(\mathbf{r})} (\nabla \times \mathbf{H}) \right) = -\varepsilon_0 \mu_0 \mu(\mathbf{r}) \frac{\partial^2 \mathbf{H}}{\partial t^2} \tag{2.14}$$

equation 2.14 becomes

$$\nabla \times \left(\frac{1}{\varepsilon(\mathbf{r})} (\nabla \times \mathbf{H}) \right) = -\frac{1}{c^2} \mu(\mathbf{r}) \frac{\partial^2 \mathbf{H}}{\partial t^2} \tag{2.15}$$

where $c = \dfrac{1}{\sqrt{\varepsilon_0 \mu_0}}$.

When $\mathbf{H}$ is a time and space dependent periodic function naturally. Writing it as harmonic modes helps us to separate the time dependency.

$$\mathbf{H}(\mathbf{r}, t) = \int_{-\infty}^{\infty} d\omega \mathbf{H}(\mathbf{r}, \omega) e^{-i\omega t} \tag{2.16}$$

Substituting it into the equation 2.15 we get,

$$\int d\omega e^{-i\omega t} \left\{ \nabla \times \left(\frac{1}{\varepsilon(\mathbf{r})} (\nabla \times \mathbf{H}(\mathbf{r}, \omega)) \right) - \frac{\omega^2}{c^2} \mu(\mathbf{r}) \mathbf{H}(\mathbf{r}, \omega) \right\} = 0 \tag{2.17}$$

In order for equation 2.17 to be true, expression in curly braces must be zero.
Now we need to deal with the periodic dielectric function $\varepsilon(\mathbf{r})$.

$$\varepsilon(\mathbf{r}) = \varepsilon(\mathbf{r} + \mathbf{R}) = \sum_{\mathbf{R}} \varepsilon(\mathbf{r} + \mathbf{R}) \tag{2.18}$$

where $\mathbf{R}$ is a lattice vector. Fourier basis of these functions which are in real space is needed to be defined. The Fourier Transform of any periodic function in the form of $f(\mathbf{r}) = f(\mathbf{r} + \mathbf{R})$ is

$$f(\mathbf{r}) = \sum_{G} f(\mathbf{G}) e^{i\mathbf{G}\cdot\mathbf{r}} \tag{2.19}$$

The periodic dielectric function becomes

$$\chi(\mathbf{r}) = \sum_{\mathbf{G}} \chi(\mathbf{G}) e^{i\mathbf{G}\cdot\mathbf{r}} \tag{2.20}$$

$$\mu(\mathbf{r}) = \sum_{\mathbf{G}} \mu(\mathbf{G}) e^{i\mathbf{G}\cdot\mathbf{r}} \tag{2.21}$$

where $\chi(\mathbf{r}) = \dfrac{1}{\varepsilon(\mathbf{r})}$ and $\mathbf{G}$ is the reciprocal lattice vector. Once more we write

$$\mathbf{H}(\mathbf{r},\omega) = \int_{-\infty}^{\infty} d\mathbf{r}' e^{i\mathbf{r}'\cdot\mathbf{r}} \mathbf{H}(\mathbf{r}',\omega) \tag{2.22}$$

So the equation 2.17 becomes

$$\begin{aligned} \nabla \times \left[\sum_{\mathbf{G}} \chi(\mathbf{G}) e^{i\mathbf{G}\cdot\mathbf{r}} \nabla \times \int d\mathbf{r}' e^{i\mathbf{r}'\cdot\mathbf{r}} \mathbf{H}(\mathbf{r}',\omega) \right] \\ - \frac{\omega^2}{c^2} \sum_{\mathbf{G}} \mu(\mathbf{G}) e^{i\mathbf{G}\cdot\mathbf{r}} \int d\mathbf{r}' e^{i\mathbf{r}'\cdot\mathbf{r}} \mathbf{H}(\mathbf{r}',\omega) = 0 \end{aligned} \tag{2.23}$$

Note that, one needs to use the given vector identity then the curl of the integral is simple,

$$\nabla \times (f\mathbf{A}) = f(\nabla \times \mathbf{A}) - \mathbf{A} \times (\nabla f) \tag{2.24}$$

$$\nabla \times \int d\mathbf{r}' e^{i\mathbf{r}'\cdot\mathbf{r}} \mathbf{H}(\mathbf{r}',\omega) = \int d\mathbf{r}' \nabla \times \left[e^{i\mathbf{r}'\cdot\mathbf{r}} \mathbf{H}(\mathbf{r}',\omega) \right] \tag{2.25}$$

$$= \int d\mathbf{r}' i\mathbf{r}' \times \mathbf{H}(\mathbf{r}',\omega) e^{i\mathbf{r}'\cdot\mathbf{r}} \tag{2.26}$$

The integral over $\mathbf{r}'$ is over the entire reciprocal space. We need to split reciprocal space into chunks in order to work in first Brillouin zone.

$$\int_{all\ \mathbf{r}'} d\mathbf{r}' f(\mathbf{r}') = \int_{cell} d\mathbf{k} \sum_{G} f(\mathbf{k}+\mathbf{G}) \tag{2.27}$$

Rewriting the equation 2.23

$$\begin{aligned} \nabla \times \left[\left(\sum_{\mathbf{G}''} \chi(\mathbf{G}'') e^{i\mathbf{G}''\cdot\mathbf{r}} \right) \left(\int d\mathbf{k} \sum_{\mathbf{G}'} i(\mathbf{k}+\mathbf{G}') \times \mathbf{H}(\mathbf{k}+\mathbf{G}',\omega) e^{i(\mathbf{k}+\mathbf{G}')\cdot\mathbf{r}} \right) \right] \\ - \frac{\omega^2}{c^2} \sum_{\mathbf{G}''} \mu(\mathbf{G}'') e^{i\mathbf{G}''\cdot\mathbf{r}} \left(\int d\mathbf{k} \sum_{\mathbf{G}'} \mathbf{H}(\mathbf{k}+\mathbf{G}',\omega) e^{i(\mathbf{k}+\mathbf{G}')\cdot\mathbf{r}} \right) = 0 \end{aligned} \tag{2.28}$$

$$\int d\mathbf{k} \sum_{\mathbf{G}''} \sum_{\mathbf{G}'} \chi(\mathbf{G}'') \nabla \times \left[i(\mathbf{k}+\mathbf{G}') \times \mathbf{H}(\mathbf{k}+\mathbf{G}', \omega) e^{i(\mathbf{k}+\mathbf{G}'+\mathbf{G}'')\cdot\mathbf{r}} \right] - \frac{\omega^2}{c^2} \left(\int d\mathbf{k} \sum_{\mathbf{G}'} \sum_{\mathbf{G}''} \mu(\mathbf{G}'') \mathbf{H}(\mathbf{k}+\mathbf{G}', \omega) e^{i(\mathbf{k}+\mathbf{G}'+\mathbf{G}'')\cdot\mathbf{r}} \right) = 0 \tag{2.29}$$

After the last curl operation,

$$\int d\mathbf{k} \sum_{\mathbf{G}''} \sum_{\mathbf{G}'} e^{i(\mathbf{k}+\mathbf{G}'+\mathbf{G}'')\cdot\mathbf{r}} \left\{ \chi(\mathbf{G}'') i(\mathbf{k}+\mathbf{G}'+\mathbf{G}'') \times [i(\mathbf{k}+\mathbf{G}') \times \mathbf{H}(\mathbf{k}+\mathbf{G}', \omega)] - \frac{\omega^2}{c^2} \mu(\mathbf{G}'') \mathbf{H}(\mathbf{k}+\mathbf{G}', \omega) \right\} = 0 \tag{2.30}$$

Using $\mathbf{G}' + \mathbf{G}'' \equiv \mathbf{G}$

$$\int d\mathbf{k} \sum_{G} e^{i(\mathbf{k}+\mathbf{G})\cdot\mathbf{r}} \left\{ \sum_{\mathbf{G}'} \chi(\mathbf{G}-\mathbf{G}')(\mathbf{k}+\mathbf{G}) \times [(\mathbf{k}+\mathbf{G}') \times \mathbf{H}(\mathbf{k}+\mathbf{G}', \omega)] + \frac{\omega^2}{c^2} \sum_{\mathbf{G}'} \mu(\mathbf{G}-\mathbf{G}') \mathbf{H}(\mathbf{k}+\mathbf{G}', \omega) \right\} = 0 \tag{2.31}$$

Using the equation 2.27 again

$$\int d\mathbf{r}' e^{i\mathbf{r}'\cdot\mathbf{r}} \left\{ \sum_{\mathbf{G}'} \chi(\mathbf{G}-\mathbf{G}')(\mathbf{k}+\mathbf{G}) \times [(\mathbf{k}+\mathbf{G}') \times \mathbf{H}(\mathbf{k}+\mathbf{G}', \omega)] + \frac{\omega^2}{c^2} \sum_{\mathbf{G}'} \mu(\mathbf{G}-\mathbf{G}') \mathbf{H}(\mathbf{k}+\mathbf{G}', \omega) \right\} = 0 \tag{2.32}$$

Once again, the above equation only true when the statement in curly braces is zero,

$$\sum_{\mathbf{G}'} \chi(\mathbf{G}-\mathbf{G}')(\mathbf{k}+\mathbf{G}) \times [(\mathbf{k}+\mathbf{G}') \times \mathbf{H}(\mathbf{k}+\mathbf{G}', \omega)] + \frac{\omega^2}{c^2} \sum_{\mathbf{G}'} \mu(\mathbf{G}-\mathbf{G}')\mathbf{H}(\mathbf{k}+\mathbf{G}', \omega) = 0 \tag{2.33}$$

And this is the H method, as an eigen value problem which is used by MPB. One need to know that there is also a method called E method(Sözüer et al. (1992)).

2.1.1. TM and TE Modes

In two dimensional cases, the eigenvalue problem can be separated into TM and TE modes. MPB allows us to calculate the modes separately for fields **H** and **E**. One can understand the separation of modes by Poynting's theorem,

$$\mathbf{S} = \mu_0(\mathbf{E} \times \mathbf{B}) \tag{2.34}$$

For example; if the propagation axis is z then the **E** field is in the xz plane and the **H** field normal to the plane.

Photonic bands are just like energy bands in condensed matter physics. The frequencies come from eigenvalue problem which are solved for unit cell $k - points$ in first Brillouin zone. The band structure is a plot of frequency versus $k - points$ and the function $\omega(\mathbf{k})$ is called $dispersion\ relation$.

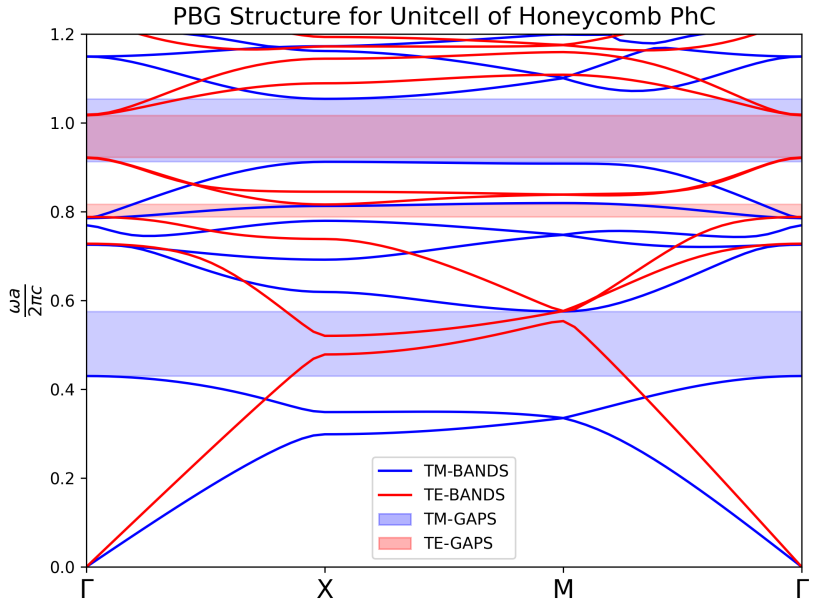

Figure 2.1. The PBG of the perfect honeycomb PhC.

2.2. Finite Difference Time Domain Method

The simulations are performed by MEEP to get the transmissions. It uses FDTD method(Taflove and Brodwin (1975); Taflove et al. (2013); Yee (1966)) so we need to understand the rate of change of the fields due to time. The idea based on chaging the infinitesimal differences(∂x , ∂y , ∂z ,) to finite differences($\triangle x$, $\triangle y$, $\triangle z$).

$$\begin{aligned} \frac{\partial \mathbf{H}}{\partial t} &= -\frac{1}{\mu_0 \mu} \nabla \times \mathbf{E} \\ \frac{\partial \mathbf{E}}{\partial t} &= \frac{1}{\varepsilon_0 \varepsilon} \left(\nabla \times \mathbf{H} - \mathbf{J}_{source} \right) \end{aligned} \tag{2.35}$$

$$\begin{aligned} \frac{\partial H_x}{\partial t} &= \frac{1}{\mu_0 \mu} \left(\frac{\partial E_y}{\partial z} - \frac{\partial E_z}{\partial y} \right) \\ \frac{\partial H_y}{\partial t} &= \frac{1}{\mu_0 \mu} \left(\frac{\partial E_z}{\partial x} - \frac{\partial E_x}{\partial z} \right) \\ \frac{\partial H_z}{\partial t} &= \frac{1}{\mu_0 \mu} \left(\frac{\partial E_x}{\partial y} - \frac{\partial E_y}{\partial x} \right) \end{aligned} \tag{2.36}$$

$$\frac{\partial E_x}{\partial t} = \frac{1}{\varepsilon_0 \varepsilon}\left(\frac{\partial H_z}{\partial y} - \frac{\partial H_y}{\partial z} - J_x\right)$$
$$\frac{\partial E_y}{\partial t} = \frac{1}{\varepsilon_0 \varepsilon}\left(\frac{\partial H_x}{\partial z} - \frac{\partial H_z}{\partial x} - J_y\right) \tag{2.37}$$
$$\frac{\partial E_z}{\partial t} = \frac{1}{\varepsilon_0 \varepsilon}\left(\frac{\partial H_y}{\partial x} - \frac{\partial H_x}{\partial y} - J_z\right)$$

Since we work in two dimensions which means our rods are infinite and uniform in z-direction. Thus, partial derivatives with respect to z must vanish

$$\frac{\partial H_x}{\partial t} = -\frac{1}{\mu_0 \mu}\frac{\partial E_z}{\partial y}$$
$$\frac{\partial H_y}{\partial t} = \frac{1}{\mu_0 \mu}\frac{E_z}{\partial x} \tag{2.38}$$
$$\frac{\partial E_z}{\partial t} = \frac{1}{\varepsilon_0 \varepsilon}\left(\frac{\partial H_y}{\partial x} - \frac{\partial H_x}{\partial y} - J_z\right)$$

Yee introduced a notation for the discretized space components $(i,\ j,\ k) = (i\triangle x,\ j\triangle y,\ k\triangle z)$ that we can define any function u in the Yee lattice (Yee (1966)).

$$u(i\triangle x,\ j\triangle y,\ k\triangle z,\ n\triangle t) = u^n_{i,\ j,\ k} \tag{2.39}$$

Partial derivatives take the forms with respect to space and time as

$$\frac{\partial u}{\partial x}(i\triangle x,\ j\triangle y,\ k\triangle z,\ n\triangle t) = \frac{u^n_{i+1/2,\ j,\ k} - u^n_{i-1/2,\ j,\ k}}{\triangle x} \tag{2.40}$$

$$\frac{\partial u}{\partial t}(i\triangle x,\ j\triangle y,\ k\triangle z,\ n\triangle t) = \frac{u^{n+1/2}_{i,\ j,\ k} - u^{n-1/2}_{i,\ j,\ k}}{\triangle t} \tag{2.41}$$

where n is an integer number and $\triangle t$ is the increment in time. Using these definitions equations 2.38 becomes

$$\frac{H_x|^{n+1/2}_{i,\,j,\,k} - H_x|^{n-1/2}_{i,\,j,\,k}}{\triangle t} = -\frac{1}{\mu_0 \mu_{i,\,j+1/2,\,k}} \frac{E_z|^{n}_{i,\,j+1/2,\,k} - E_z|^{n}_{i,\,j-1/2,\,k}}{\triangle y}$$

$$\frac{H_y|^{n+1/2}_{i,\,j,\,k} - H_y|^{n-1/2}_{i,\,j,\,k}}{\triangle t} = \frac{1}{\mu_0 \mu_{i+1/2,\,j,\,k}} \frac{E_z|^{n}_{i+1/2,\,j,\,k} - E_z|^{n}_{i-1/2,\,j,\,k}}{\triangle x} \tag{2.42}$$

$$\frac{E_z|^{n+1/2}_{i,\,j,\,k} - E_y|^{n-1/2}_{i,\,j,\,k}}{\triangle t} = \frac{1}{\varepsilon_0 \varepsilon_{i+1/2,\,j+1/2,\,k}}$$

$$\left(\frac{H_y|^{n}_{i+1/2,\,j,\,k} - H_y|^{n}_{i-1/2,\,j,\,k}}{\triangle x} - \frac{H_x|^{n}_{i,\,j+1/2,\,k} - H_x|^{n}_{i,\,j-1/2,\,k}}{\triangle y} - J_z|_{i+1/2,\,j+1/2,\,k} \right) \tag{2.43}$$

These forms of equations help us to determine vector fields at any lattice point and at any time.

2.2.1. Transmission

MEEP uses current sources in separable form in space and time as

$$\mathbf{J}(\mathbf{x}, t) = \mathbf{A}(\mathbf{x}) \cdot f(t) \tag{2.44}$$

$$\mathbf{A}(\mathbf{x}) = e_l \delta(\mathbf{x} - \mathbf{x}_0) \tag{2.45}$$

$$f(t) = (-i\omega)^{-1} \frac{\partial}{\partial t} \exp\left(\frac{-i\omega t - (t - t_0)^2}{2\omega^2} \right) \tag{2.46}$$

is the Gaussian-pulse source used for calculation of transmission($e_l : l = 1, 2, 3$ unit vectors). Incoming wave from the source strikes the PhC structure in the propagation direction $+x$. The flux spectrum is calculated by a monitor called $flux\ region$ which collects the incoming fields at the end of the structure. There is also PML(Perfectly Matched Layer)(Berenger (1994)) that absorbs EM waves without any reflection at the

boundaries of the computational cells. Presence of the PML eliminates the effects of reflections allowing us to use a relatively small cell and thus saves plenty of computational time.

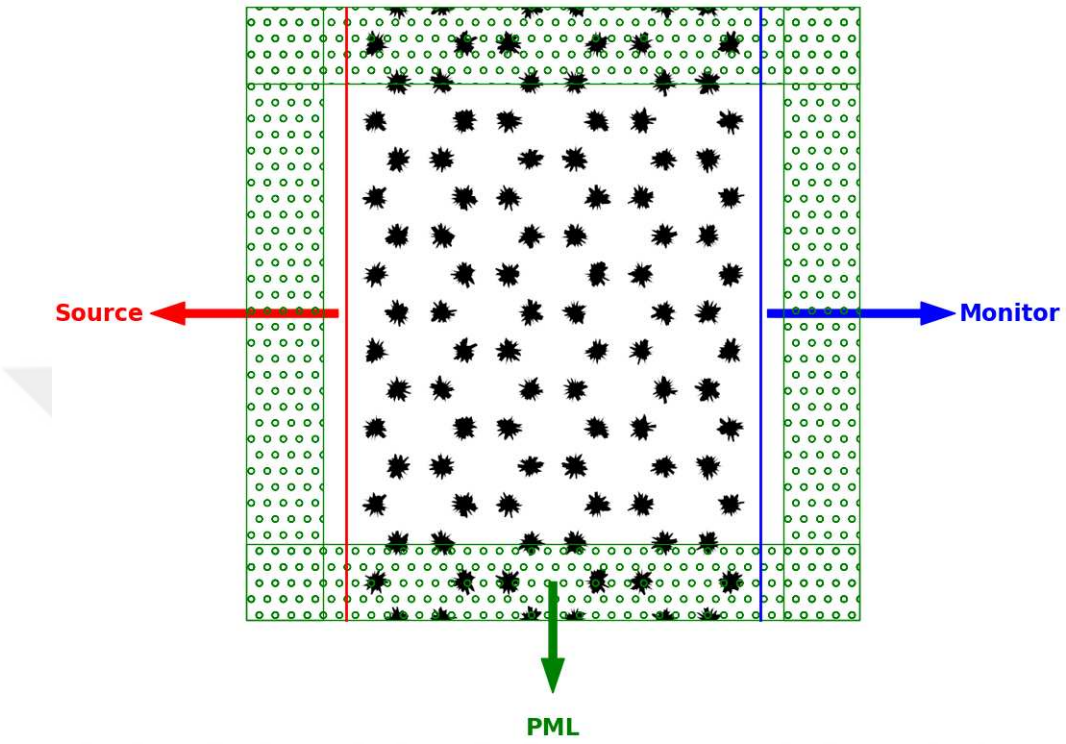

Figure 2.2. FDTD simulation cell for computation of transmission.

2.3. Supercell Method and Density of States

In the manufacturing process of PhCs, numerous errors in geometry, defects or contaminations in dielectric materials may coexist randomly on the whole crystal. Understanding the effects of these random imperfections requires a bigger cell to work on rather than one unit cell. At this point, the Supercell method must be used(Meade et al. (1991, 1993)). It is actually Plane Wave Expansion method but instead of unit cell, supercell is periodic. It is a valid method for such calculations. MPB easily allows to switch between the unit cell and the supercell.

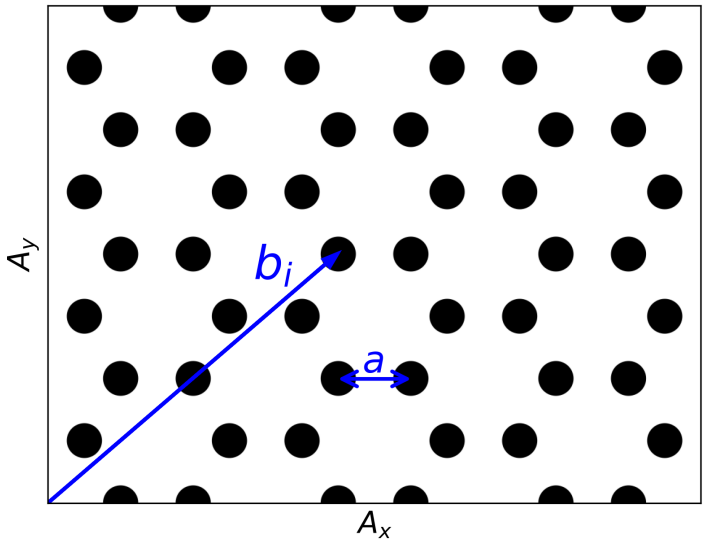

Figure 2.3. A 2D supercell of a perfect honeycomb PhC with dimensions $A_x = 9a$ and $A_y = 4a\sqrt{3}$. Radius of rods $R = 0.24a$ with $\varepsilon_{diel} = 12$. b_i are the positions of rods.

The derivation of $\varepsilon(\mathbf{G})$ for the supercell is needed to be defined. Starting with

$$\varepsilon(\mathbf{r}) = \varepsilon_{diel} + (\varepsilon_{air} - \varepsilon_{diel}) \sum_i \Omega(R - |\mathbf{r} - \mathbf{r}_i)|) \tag{2.47}$$

where Ω is a step function. For the perfect structure we can write as

$$\varepsilon(\mathbf{G}) = \frac{1}{V_{SC}} \int_{SC} \varepsilon(\mathbf{r}) e^{-i(\mathbf{G}\cdot\mathbf{r})} d\mathbf{r} \tag{2.48}$$

$$= \varepsilon_{diel}\delta_{\mathbf{G}0} + (\varepsilon_{air} - \varepsilon_{diel}) \sum_i 2\cos(\mathbf{G}\cdot\mathbf{b}_i) \frac{J_1(GR)}{GR} \left(\frac{\pi R^2}{V_{SC}}\right) \tag{2.49}$$

and J_1 is Bessel function of the first kind. When randomness takes place dielectric function for supercell becomes

$$\varepsilon(\mathbf{G}) = \frac{1}{V_{SC}} \int_{SC} \varepsilon(\mathbf{r}) e^{-i(\mathbf{G}\cdot\mathbf{r})} d\mathbf{r} \tag{2.50}$$

$$= \varepsilon_{diel}\delta_{\mathbf{G}0} + (\varepsilon_{air} - \varepsilon_{diel}) \sum_i e^{i\mathbf{G}\cdot\mathbf{b}_i} \frac{J_1(GR)}{GR} \left(\frac{\pi R^2}{V_{SC}}\right) \tag{2.51}$$

Once a totally asymmetric supercell is used, frequencies must be calculated for all $k - points$. However, it takes enormous amount of resources. Choosing reasonable number of $k - points$ randomly over the supercell is a valid method. In our case, we used one hundered $k - points$. First two hundered band frequencies calculated for each random $k - points$ over the supercells to generate DOS for the TM modes and the TE modes. The definition of density of states (DOS) is given by the books Economou (2006); Lagendijk and Van Tiggelen (1996); Taflove et al. (2013) as

$$\text{DOS}(\omega) = \sum_n \delta(\omega - \omega_n) \tag{2.52}$$

Basicly, how many times we encountered with the same frequency at the end of calculations.

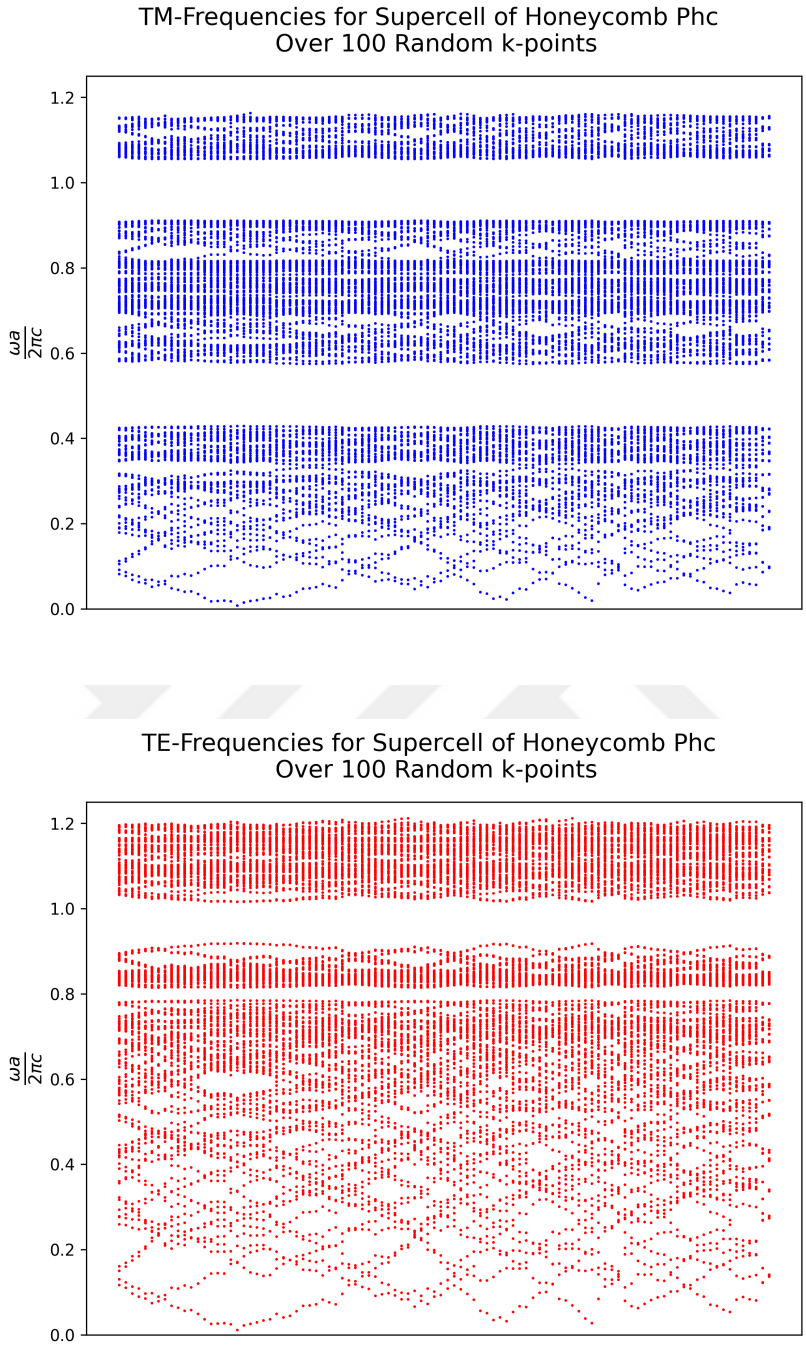

Figure 2.4. TM and TE frequencies calculated for supercell of perfect honeycomb PhC over one hundered random $k - points$.

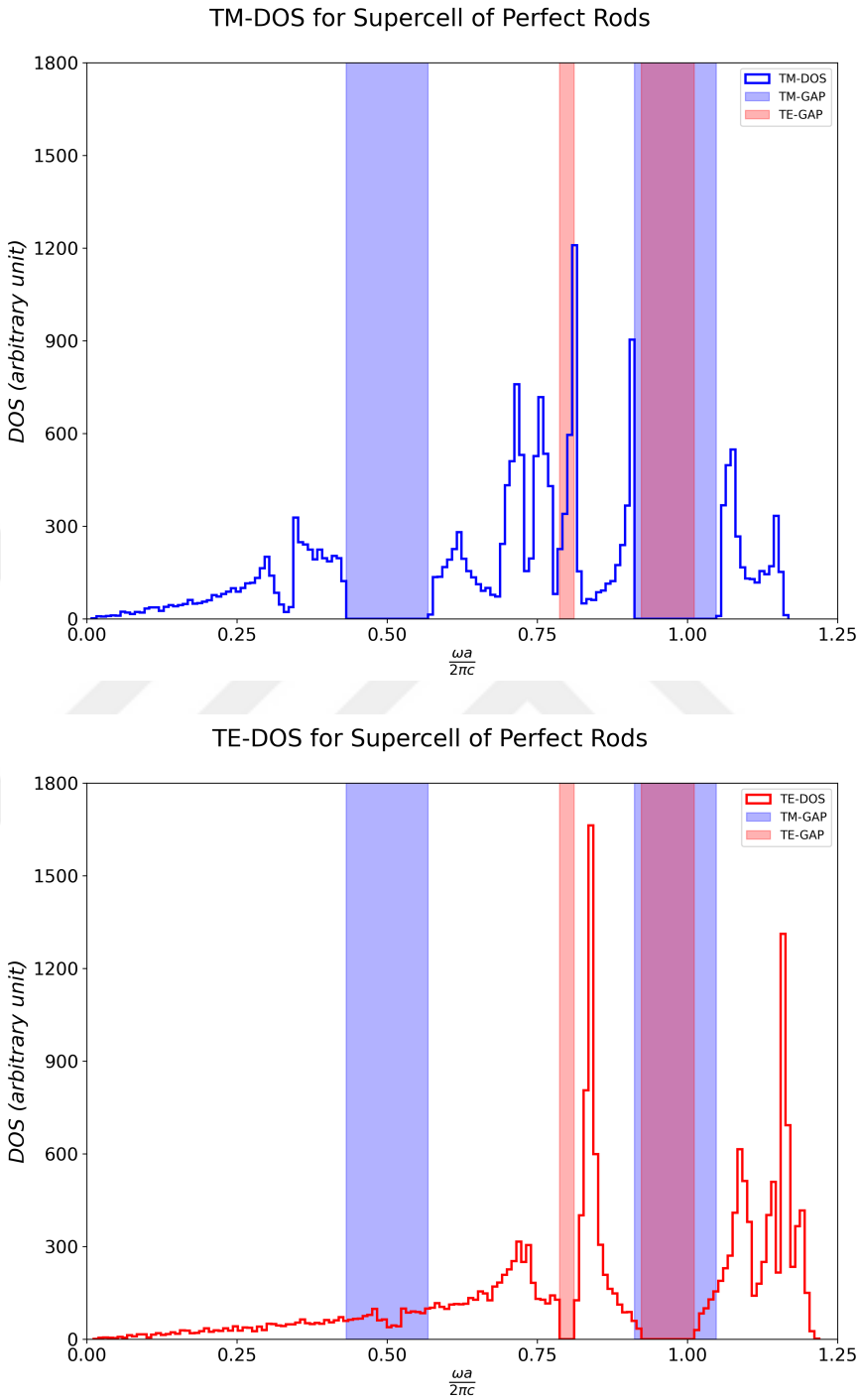

Figure 2.5. TM and TE DOS for supercell of perfect honeycomb PhC.

2.4. Numerical Considerations

MPB calculates the frequencies iteratively over eigenvectors. At the first $k-point$ randomly chosen eigenvectors are used then the minimization takes place to get each of the eigenvalues(ω). For the second $k-point$, the last eigenvectors which are used for the last step of the minimization are used as an initial guess to save time. Because of the idea that they will be very close to each other (true eigenvectors) and shorten the minimization time for the next true eigenvalue. In our case, $k-points$ are uniformly randomly distributed on the computational cell which means we can not take the advantage of the method that MPB uses. However, there must be a solving order of these $k-points$ that it takes less time to solve rather than solving randomly. This problem is actually called "Route inspection problem". The way we handled this issue is quite primitive but effective enough. Starting from a seed point the algorithm searches for the nearest $k-point$ and solves it. Then, the new seed point becomes the last $k-point$ algorithm solved and it searches again the nearest one. By this technique we achieved to save time up to 40% in average against randomly ordered $k-points$.

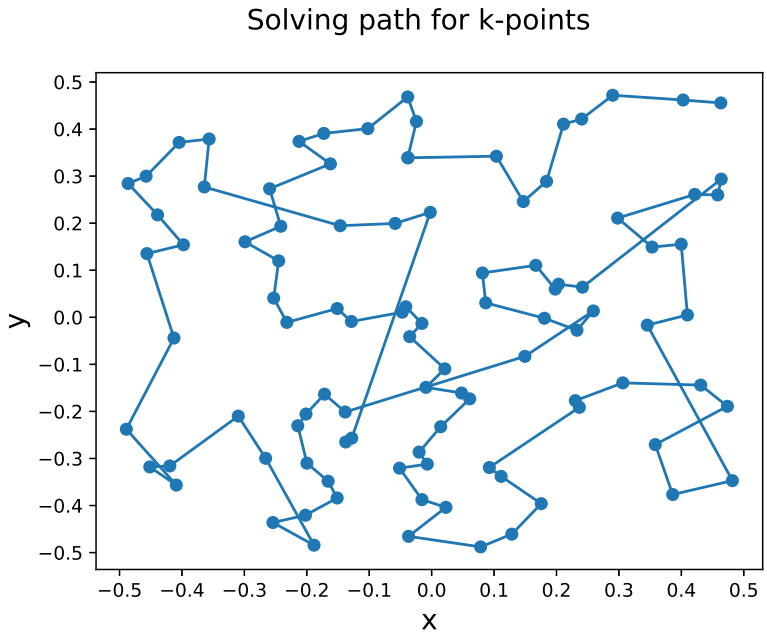

Figure 2.6. Simple demonstration of solving path for random one hundred $k-points$.

CHAPTER 3

IMPERFECT PHOTONIC CRYSTAL

Imperfections may occur in various ways. Most often, these random errors occur during the manufacturing process. We can easily narrow down those random errors into two types for our problem: rods with only rough surfaces and randomly positioned rods with rough surfaces in honeycomb lattice structure. Starting from the perfect crystal, we deformed the surfaces of the rods randomly but in a systematic way. Besides, we randomly shifted the positions of the rods with surface roughness.

3.1. Creating Surface Roughness and Positional Randomness

Uniformly distributed fifty random numbers in a given interval are used while deforming the surface of a single rod. The limits of that interval (3.2) are decided by the percentage of the randomness depended on the perfect rod radius r.

$$\kappa : 10, 20, 30, 40, 45 \tag{3.1}$$

$$\{r' : -\frac{\kappa r}{100} \leq r' \leq \frac{\kappa r}{100}\} \tag{3.2}$$

These random numbers are simply added to the radius r to generate the new sets of coordinate points x, y which determined the deformed surface.

$$x = (r' + r)\cos(\theta) \tag{3.3}$$

$$y = (r' + r)\sin(\theta) \tag{3.4}$$

We also investigated the condition that two possible error types coexist; positional randomness and surface roughness. A set of uniformly random numbers for the centers of

the rods are used during mispacing. This set choosen from an area of a disk whose radius determined by the percentage of nearest neighbor distance.

$$\nu : 10, 20, 30 \tag{3.5}$$

$$\rho = \frac{\nu a}{100} \tag{3.6}$$

$$\{x : -\rho \leq x \leq \rho\} \tag{3.7}$$

$$\{y : -\rho \leq y \leq \rho\} \tag{3.8}$$

$$\{C(x, y) : x^2 + y^2 \leq \rho^2\} \tag{3.9}$$

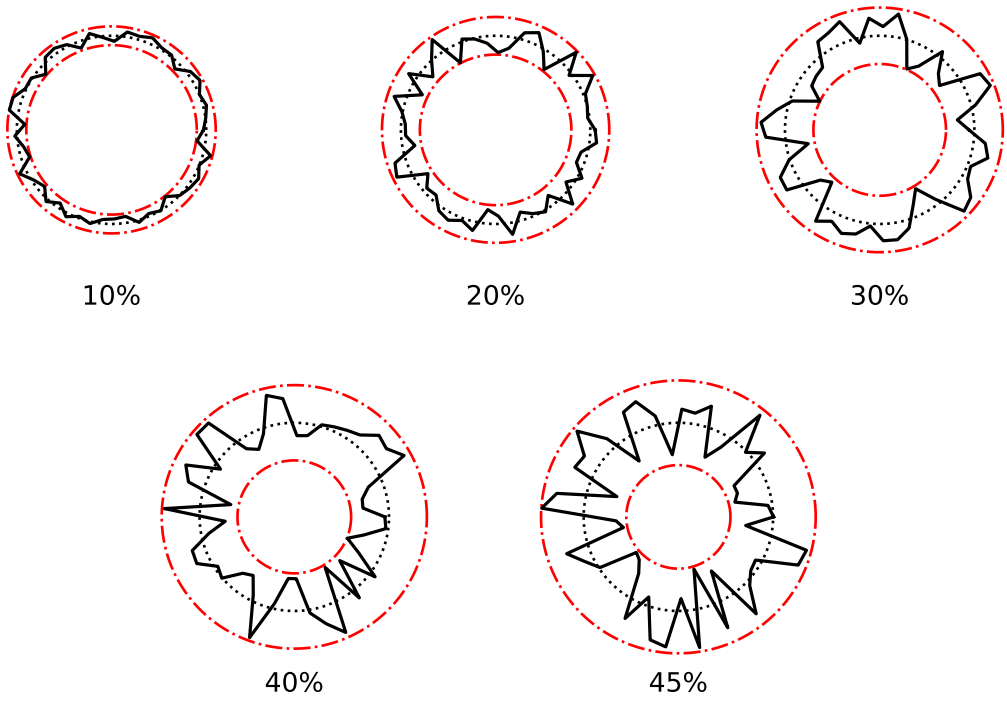

Figure 3.1. Rough surface illustrations of rods for given percentages. Black dotted circles indicates perfect rod surfaces. Red dashed dotted lines are limits of r' and black lines are rough surfaces.

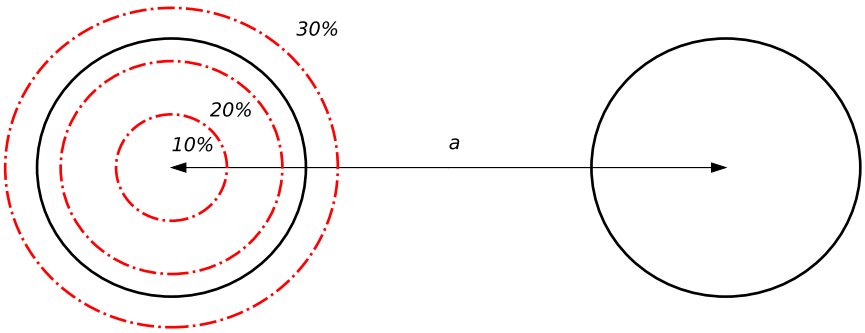

Figure 3.2. Red dashed dotted lines are allowed limits for centers of deformed rods to be placed. a is the nearest neighbour distance.

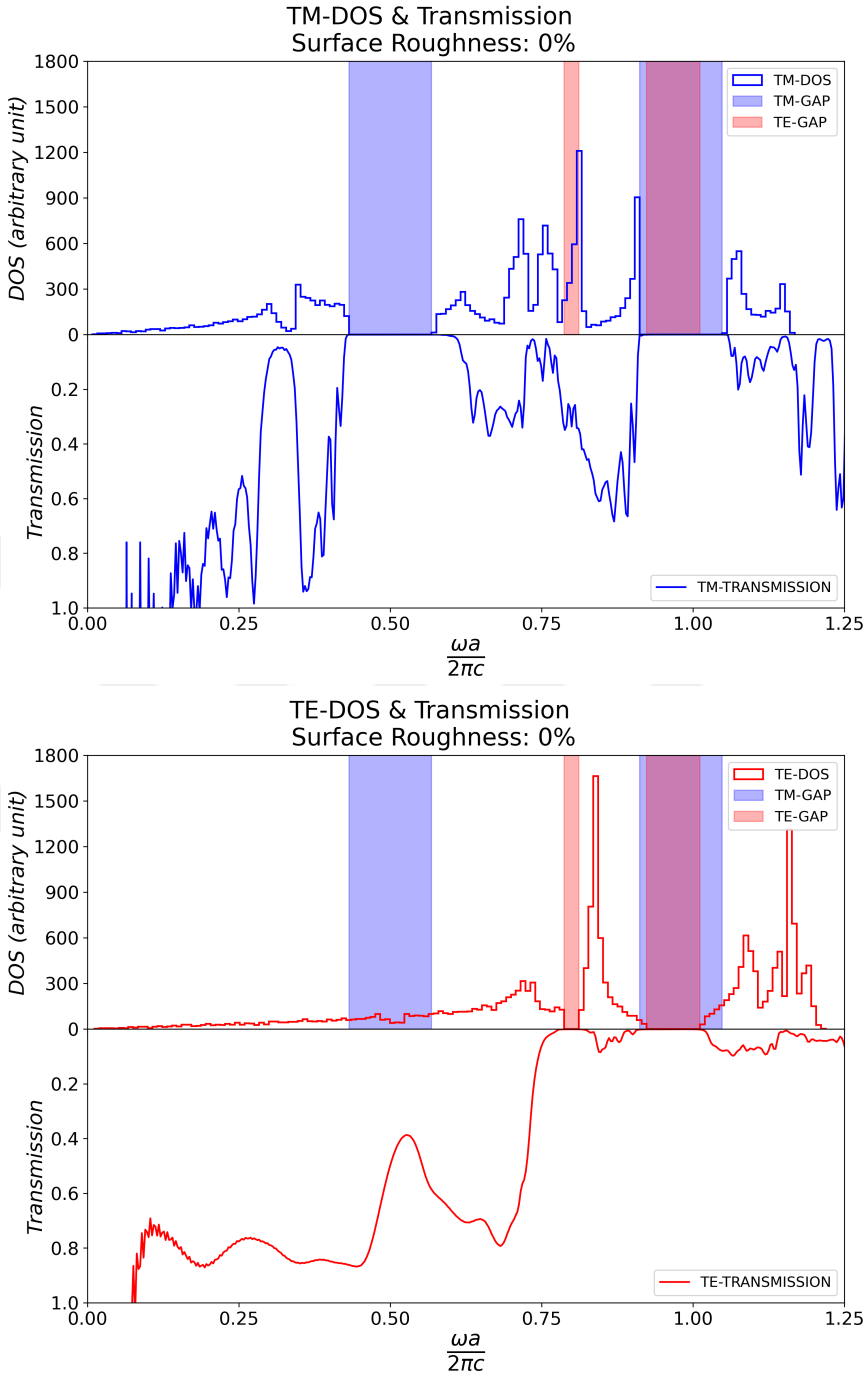

Figure 3.3. The DOS of the TM modes, TE modes over one hundered random $k - points$ and the transmission for the perfect honeycomb PhC.

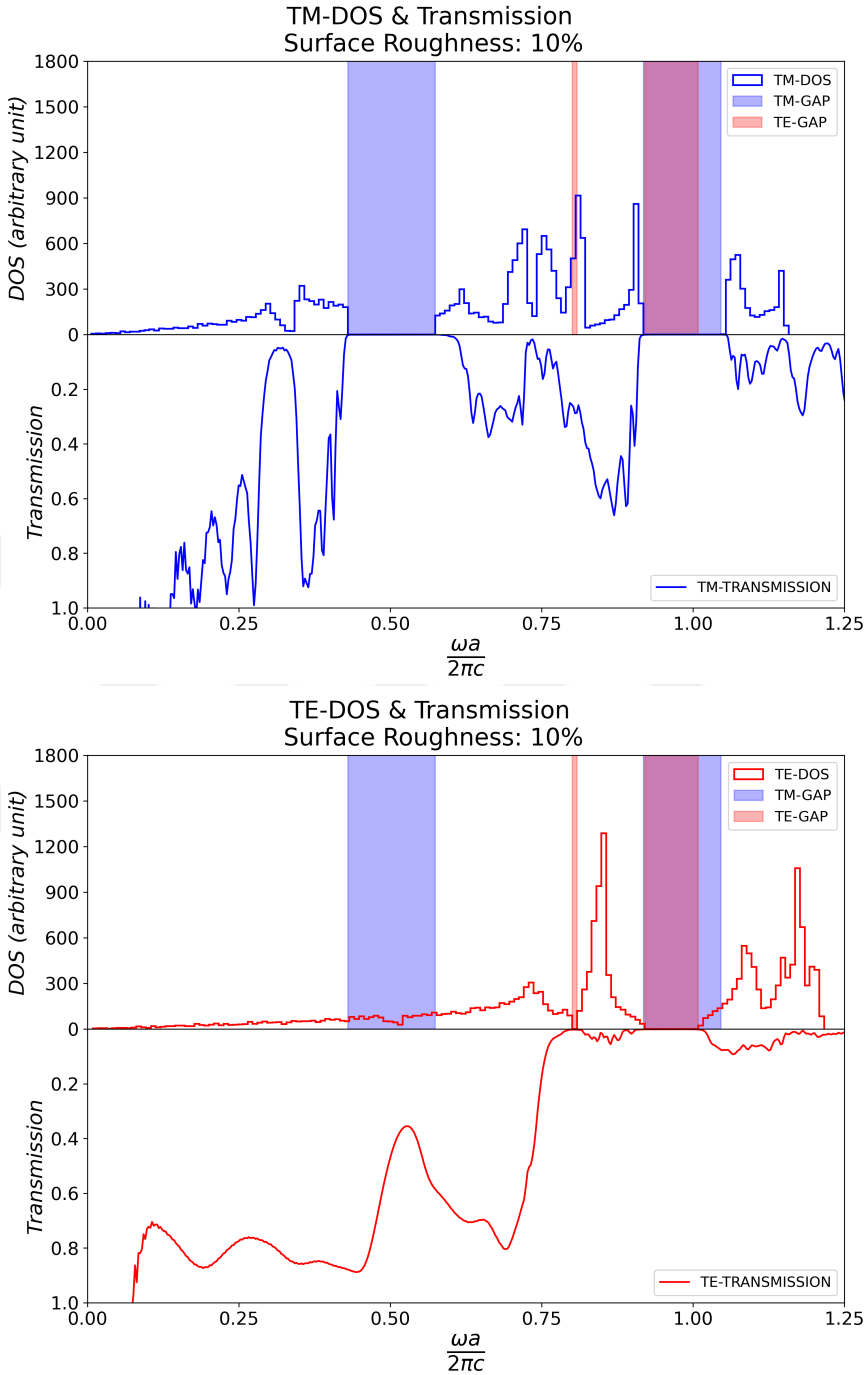

Figure 3.4. The DOS of the TM modes, TE modes over one hundered random $k - points$ and the transmission for the 10% surface roughness.

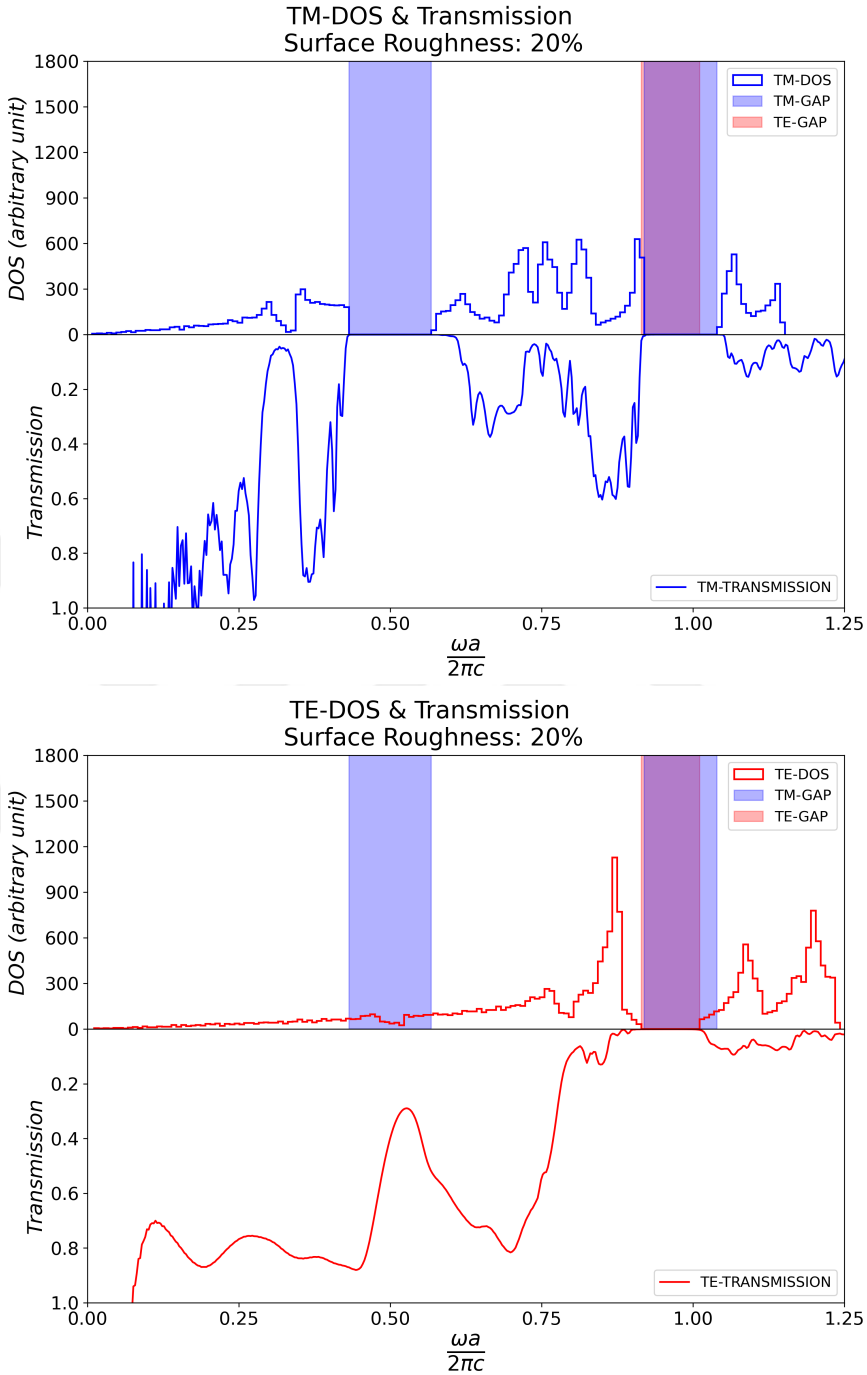

Figure 3.5. The DOS of the TM modes, TE modes over one hundered random $k - points$ and the transmission for the 20% surface roughness.

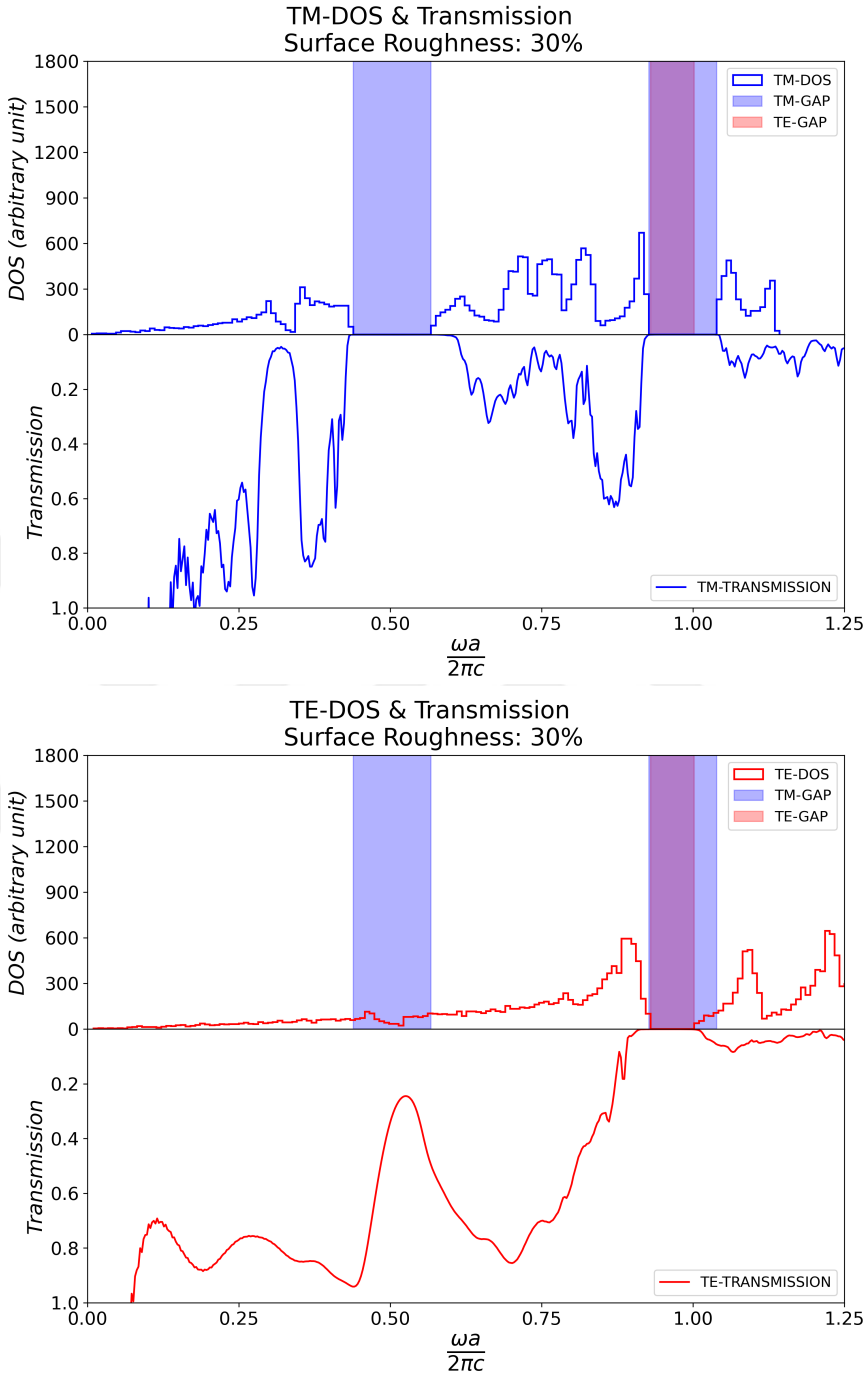

Figure 3.6. The DOS of the TM modes, TE modes over one hundered random $k - points$ and the transmission for the 30% surface roughness.

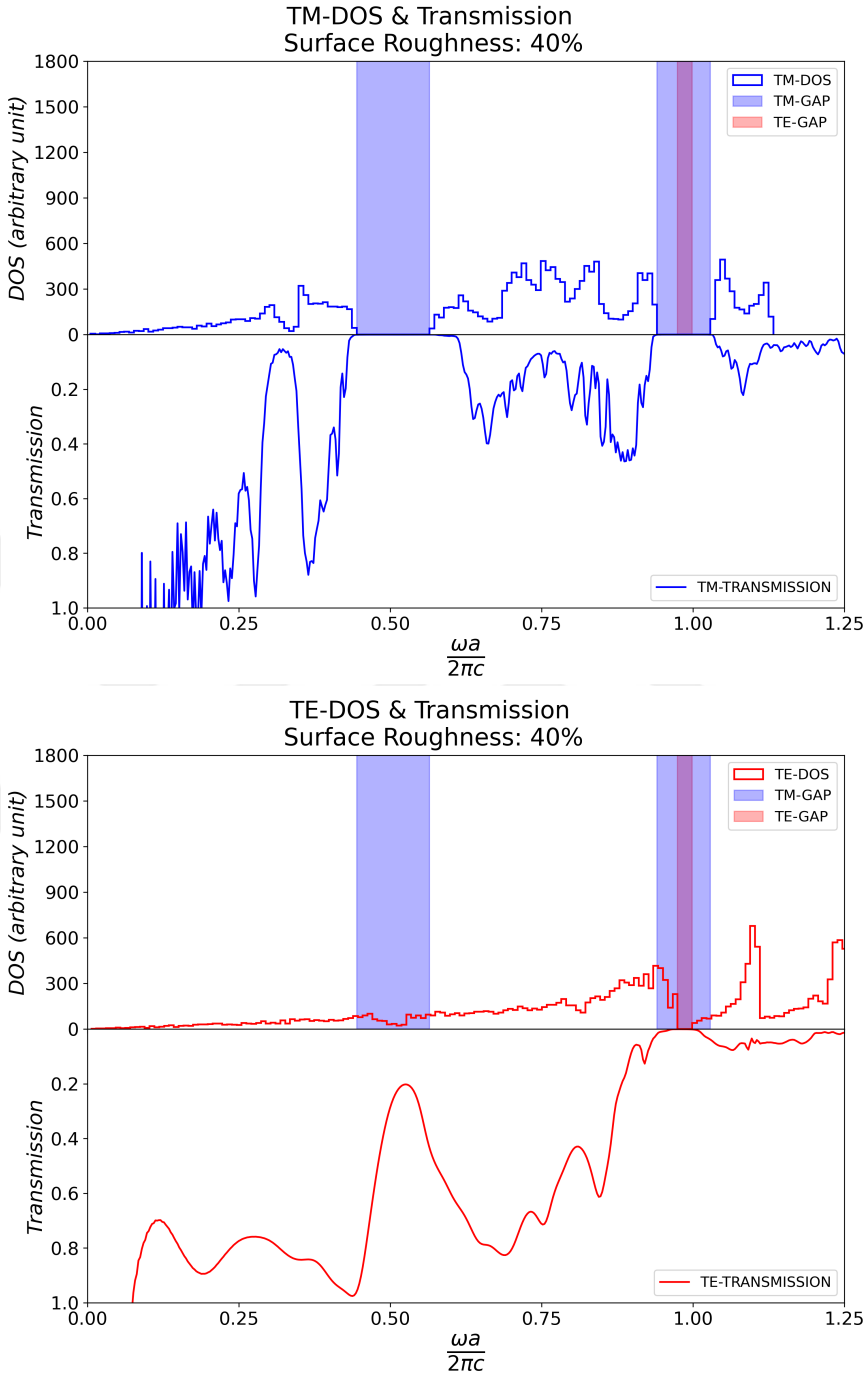

Figure 3.7. The DOS of the TM modes, TE modes over one hundered random $k - points$ and the transmission for the 40% surface roughness.

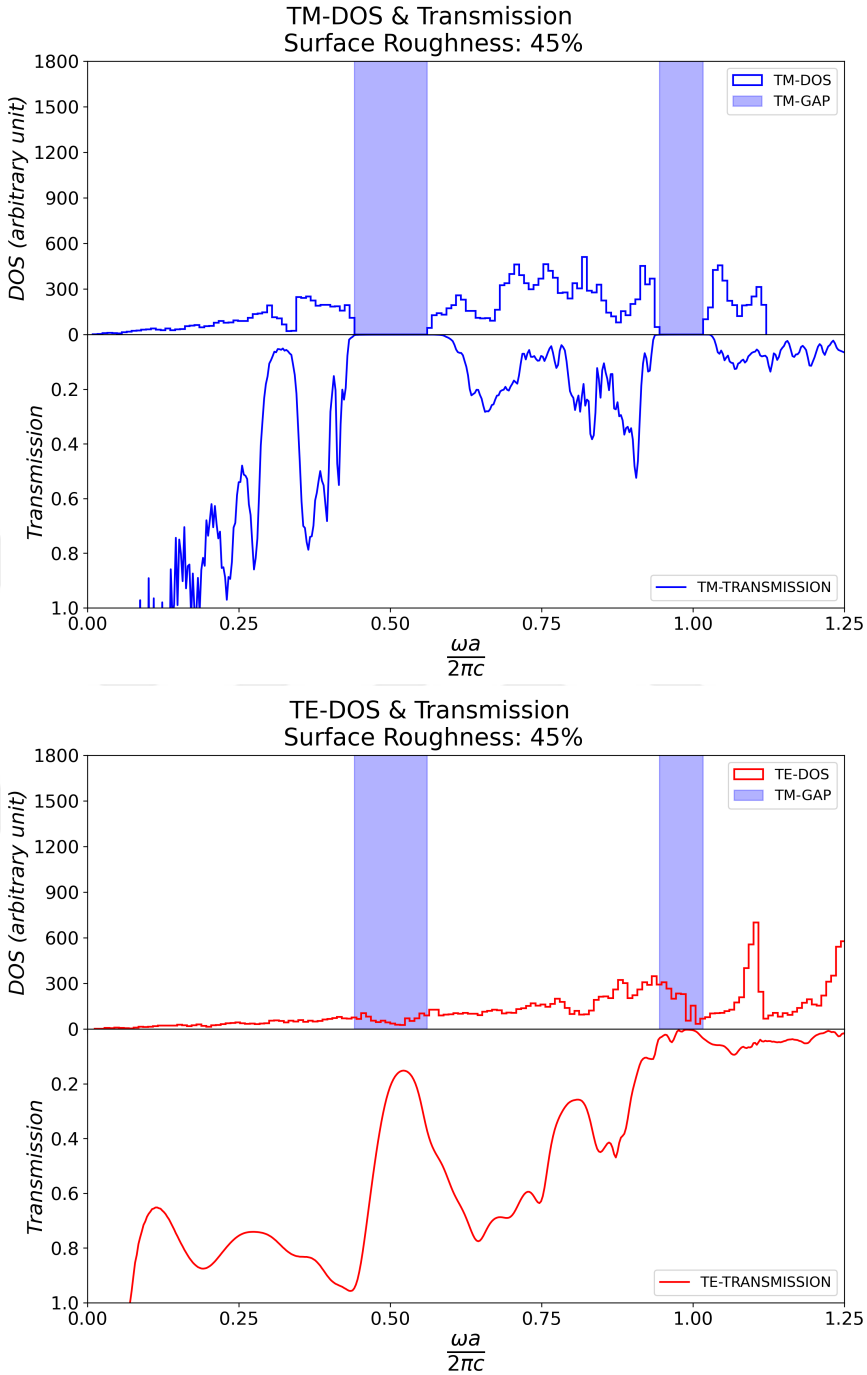

Figure 3.8. The DOS of the TM modes, TE modes over one hundered random $k - points$ and the transmission for the 45% surface roughness.

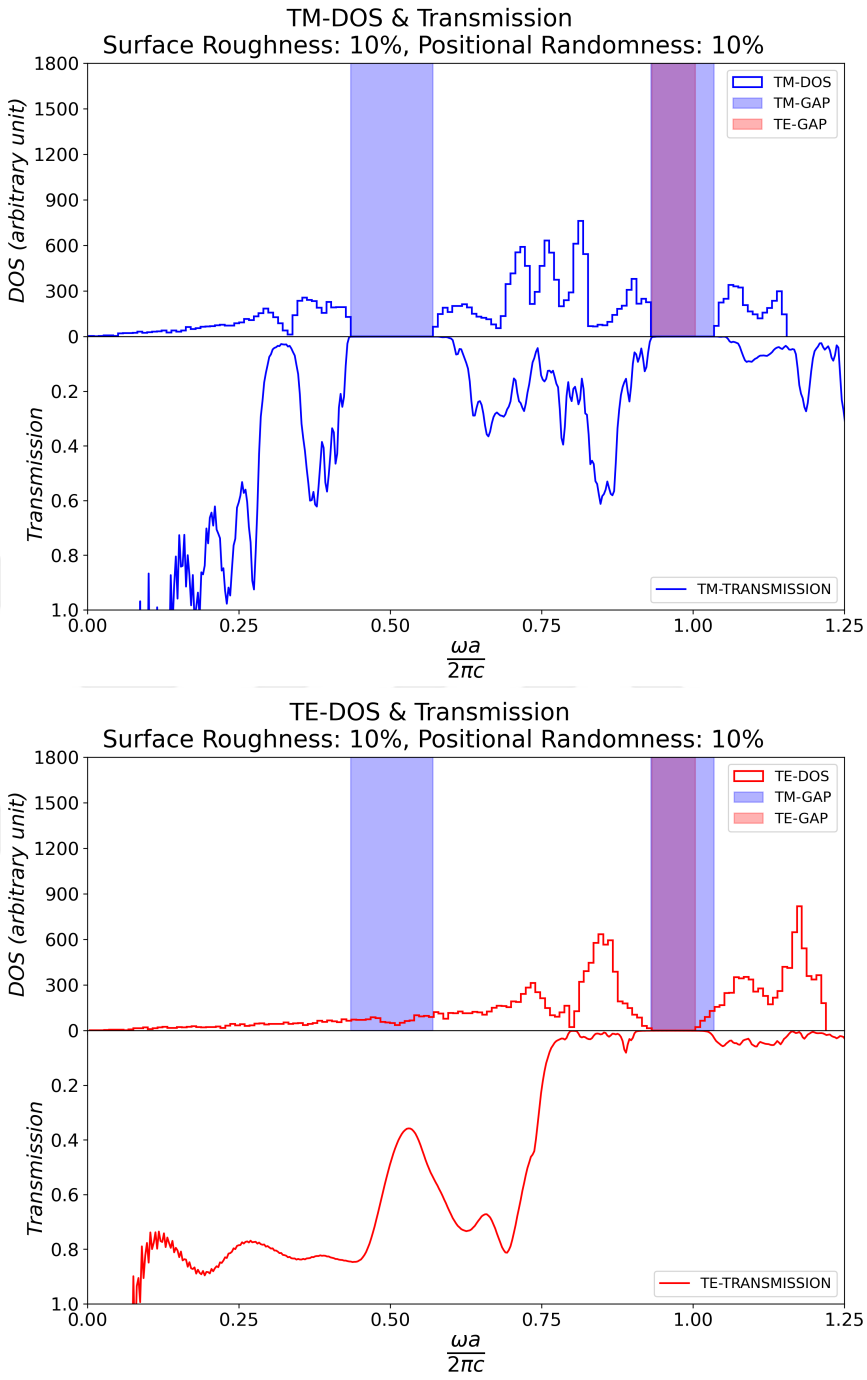

Figure 3.9. The DOS of the TM modes, TE modes over one hundered random $k - points$ and the transmission for the 10% surface roughness and 10% positional randomness.

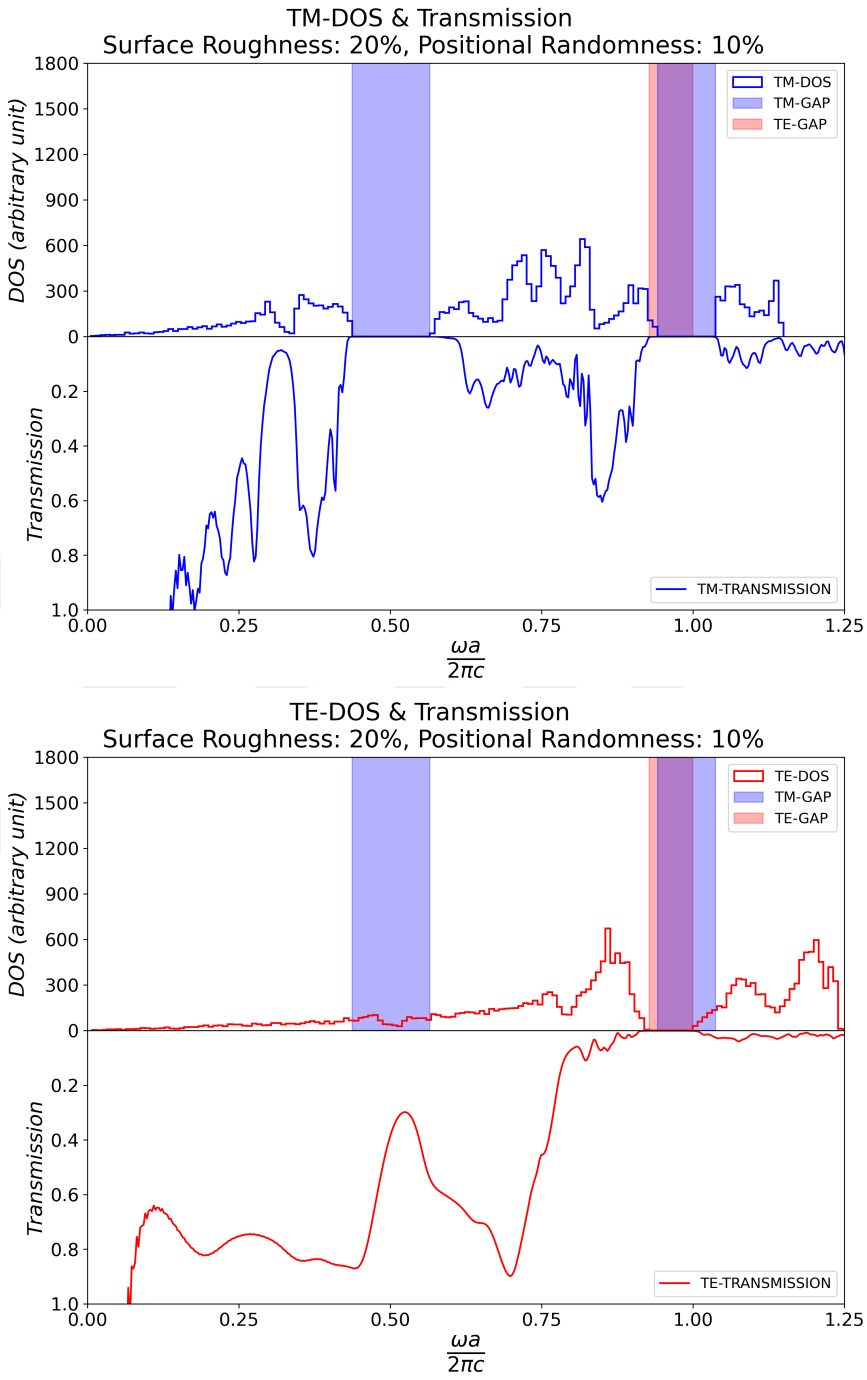

Figure 3.10. The DOS of the TM modes, TE modes over one hundered random $k-points$ and the transmission for the 20% surface roughness and 10% positional randomness.

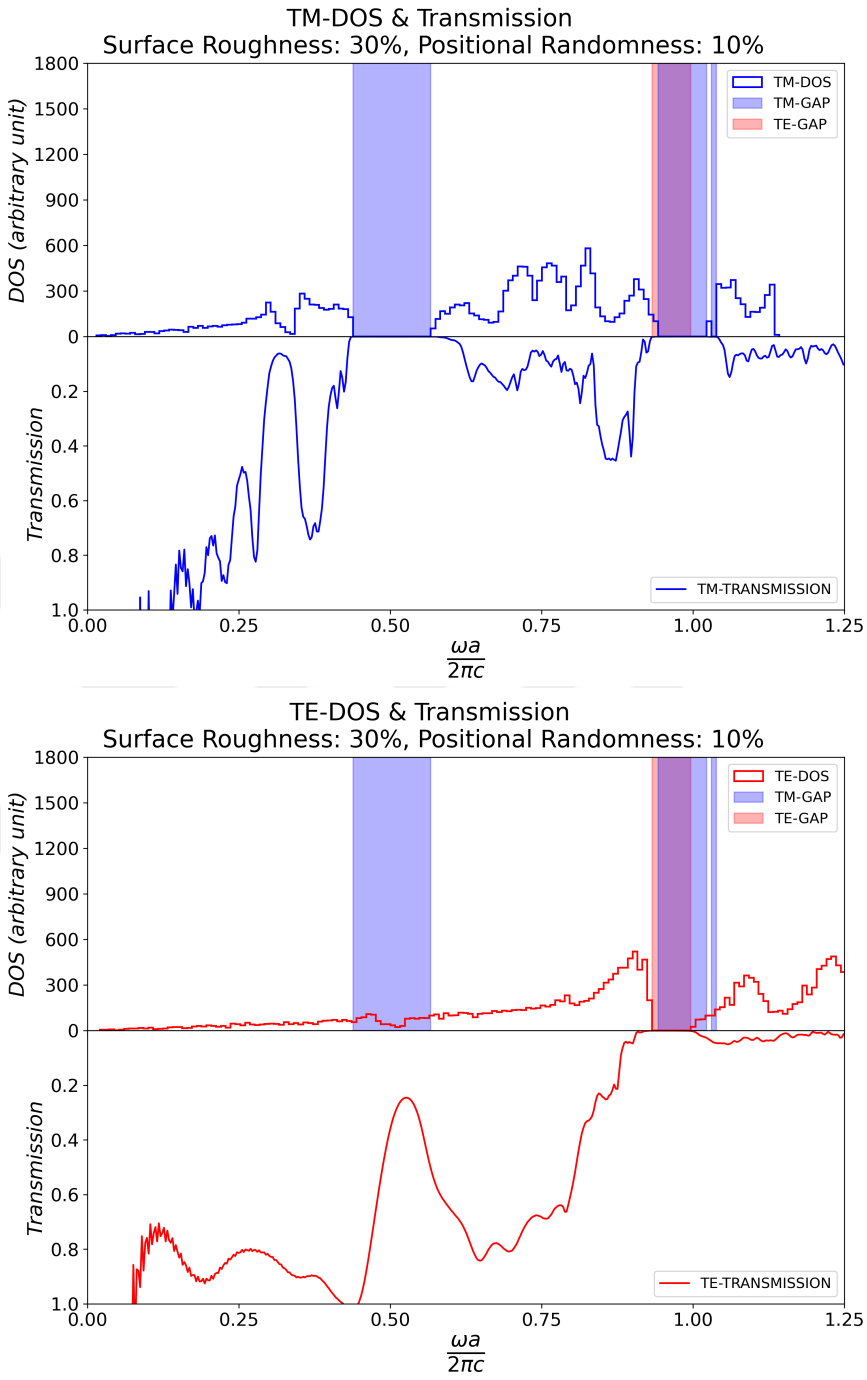

Figure 3.11. The DOS of the TM modes, TE modes over one hundered random $k - points$ and the transmission for the 30% surface roughness and 10% positional randomness.

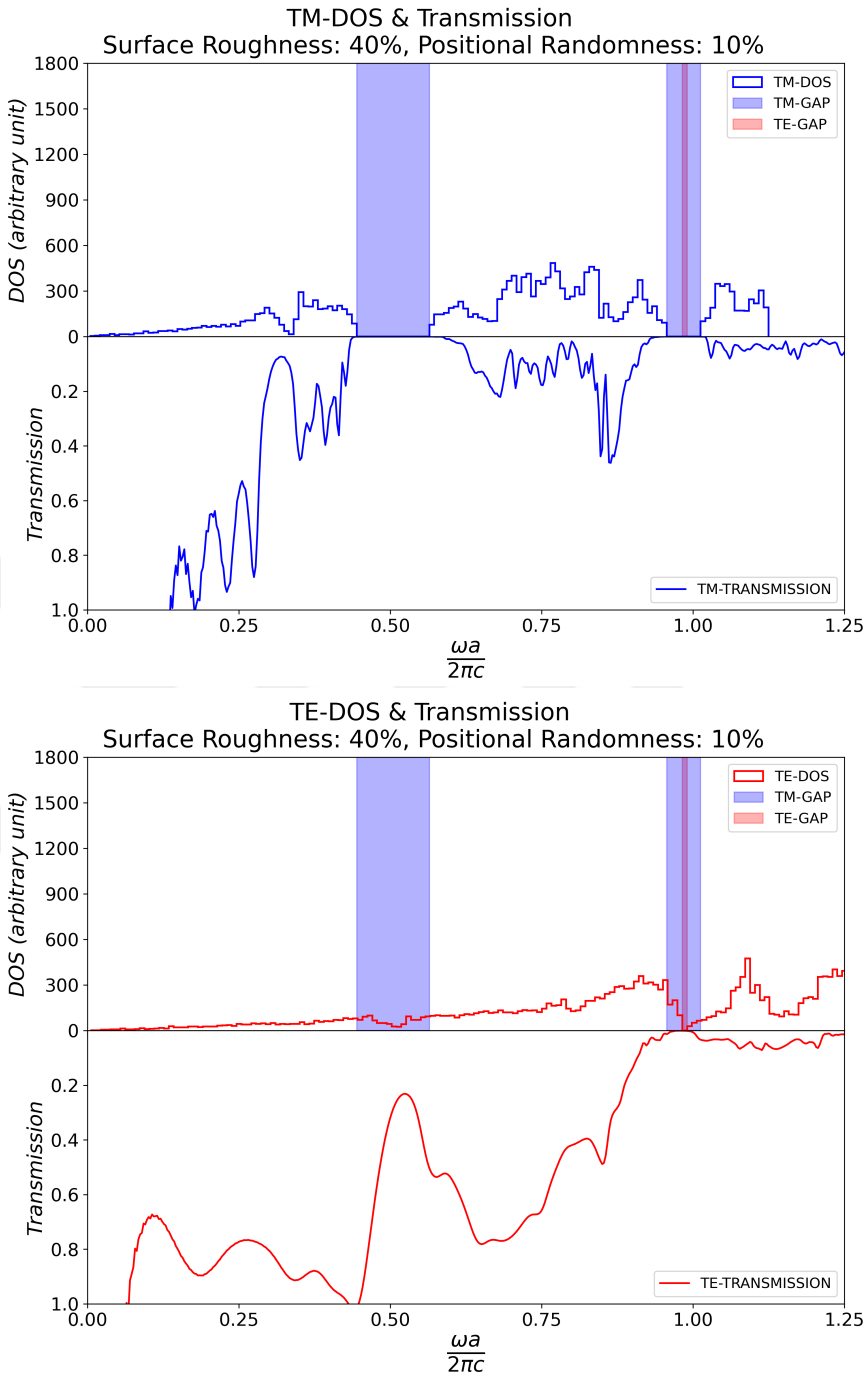

Figure 3.12. The DOS of the TM modes, TE modes over one hundered random $k-points$ and the transmission for the 40% surface roughness and 10% positional randomness.

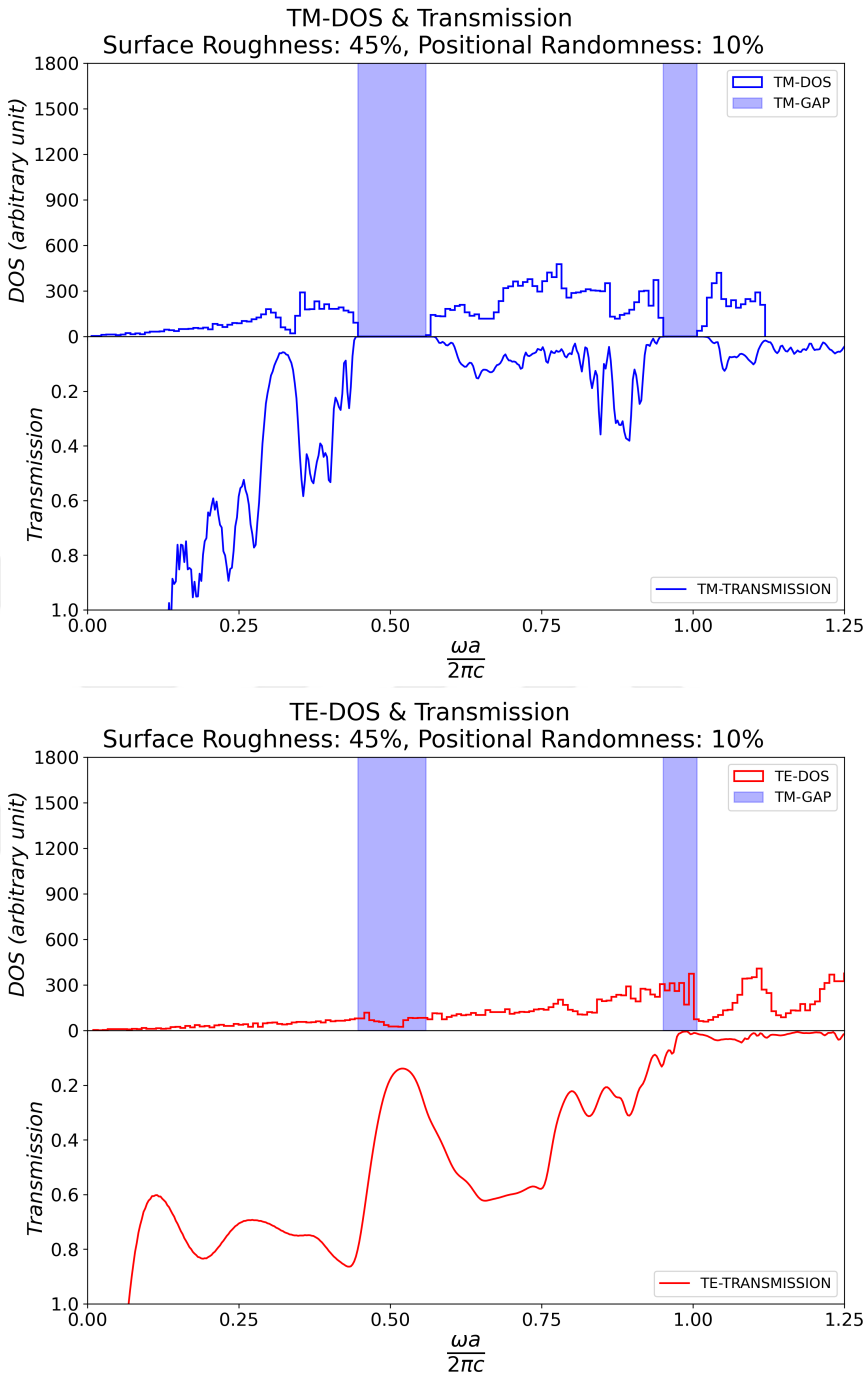

Figure 3.13. The DOS of the TM modes, TE modes over one hundered random $k-points$ and the transmission for the 45% surface roughness and 10% positional randomness.

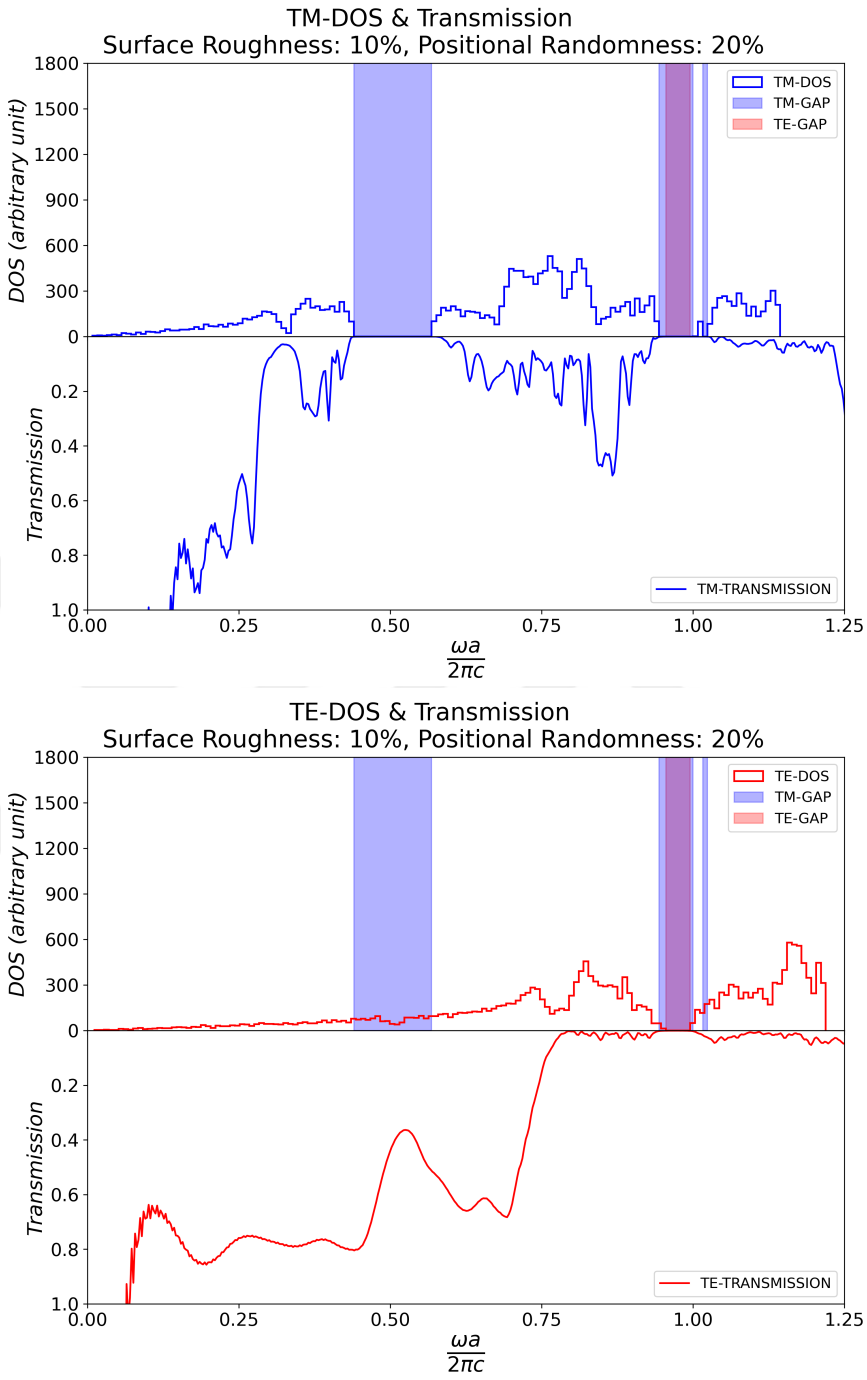

Figure 3.14. The DOS of the TM modes, TE modes over one hundered random $k - points$ and the transmission for the 10% surface roughness and 20% positional randomness.

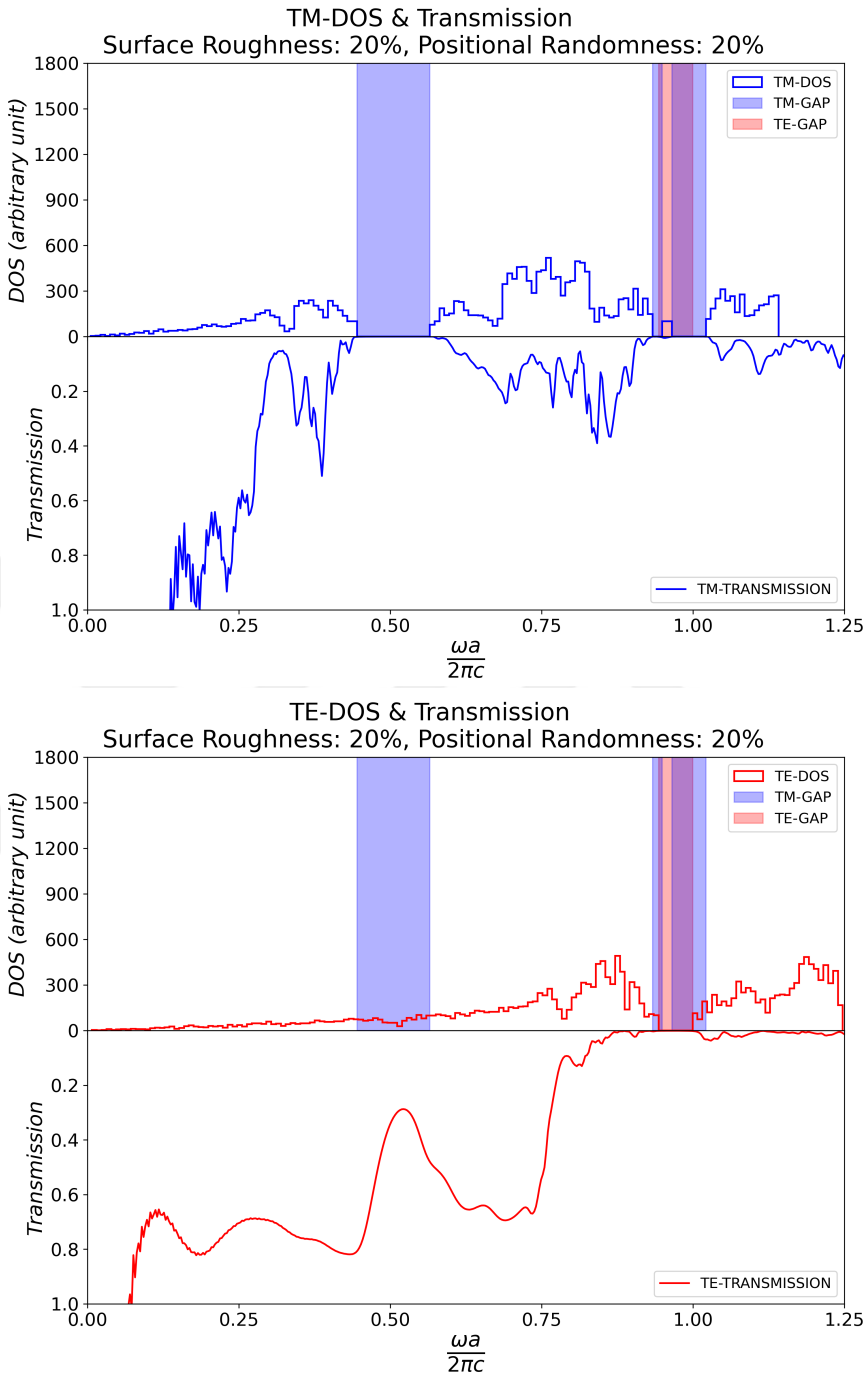

Figure 3.15. The DOS of the TM modes, TE modes over one hundered random $k - points$ and the transmission for the 20% surface roughness and 20% positional randomness.

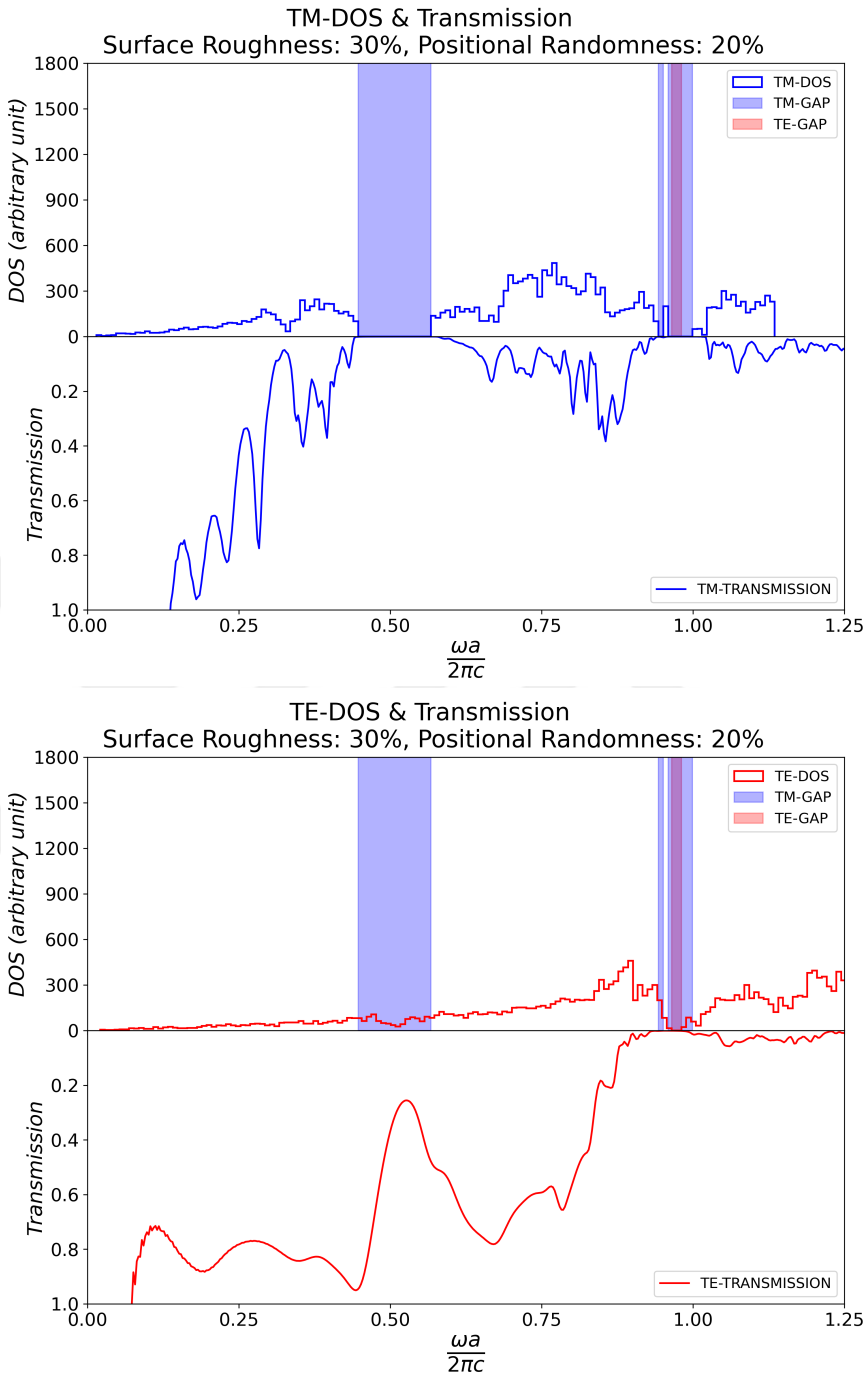

Figure 3.16. The DOS of the TM modes, TE modes over one hundered random $k - points$ and the transmission for the 30% surface roughness and 20% positional randomness.

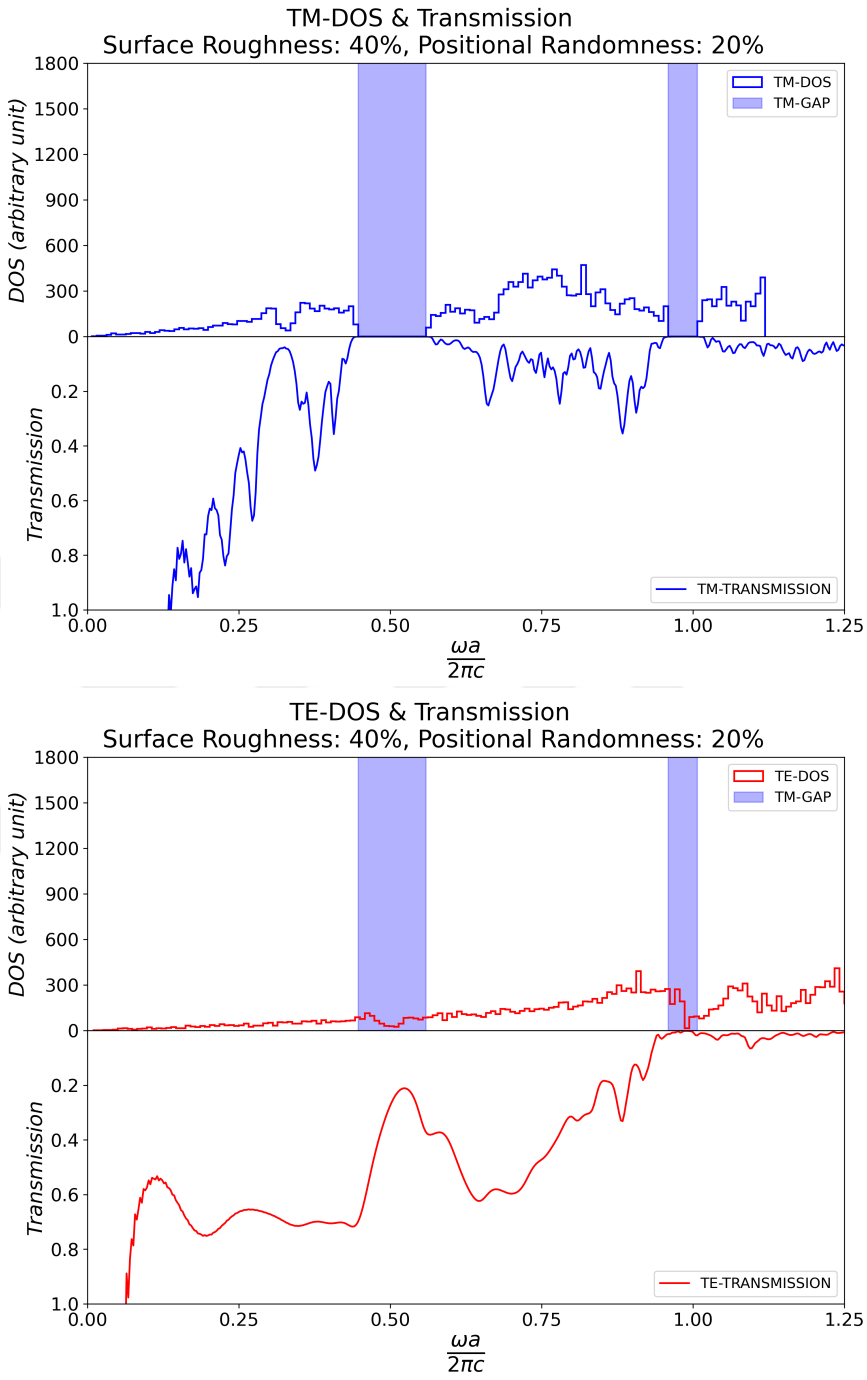

Figure 3.17. The DOS of the TM modes, TE modes over one hundered random $k-points$ and the transmission for the 40% surface roughness and 20% positional randomness.

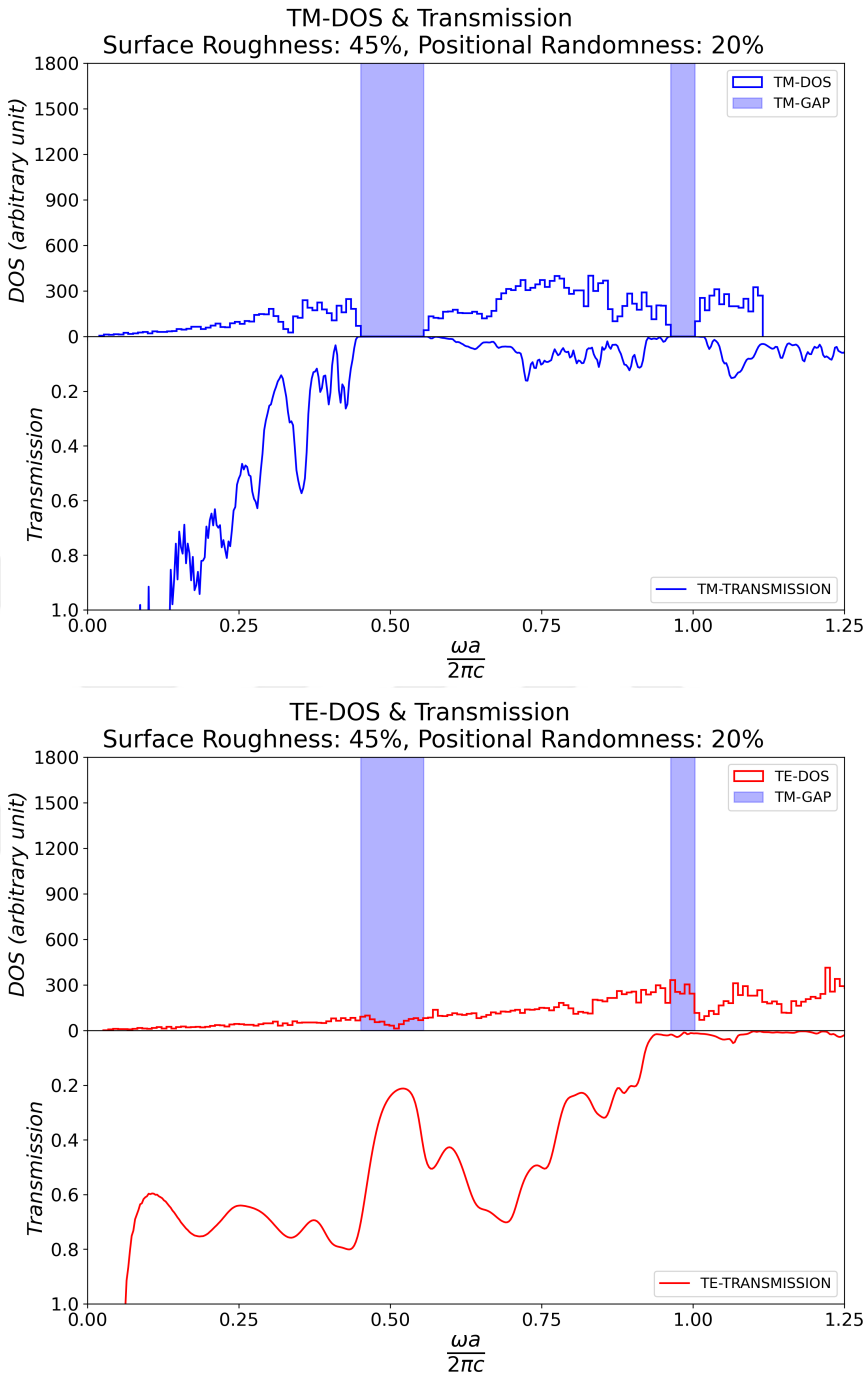

Figure 3.18. The DOS of the TM modes, TE modes over one hundered random $k - points$ and the transmission for the 45% surface roughness and 20% positional randomness.

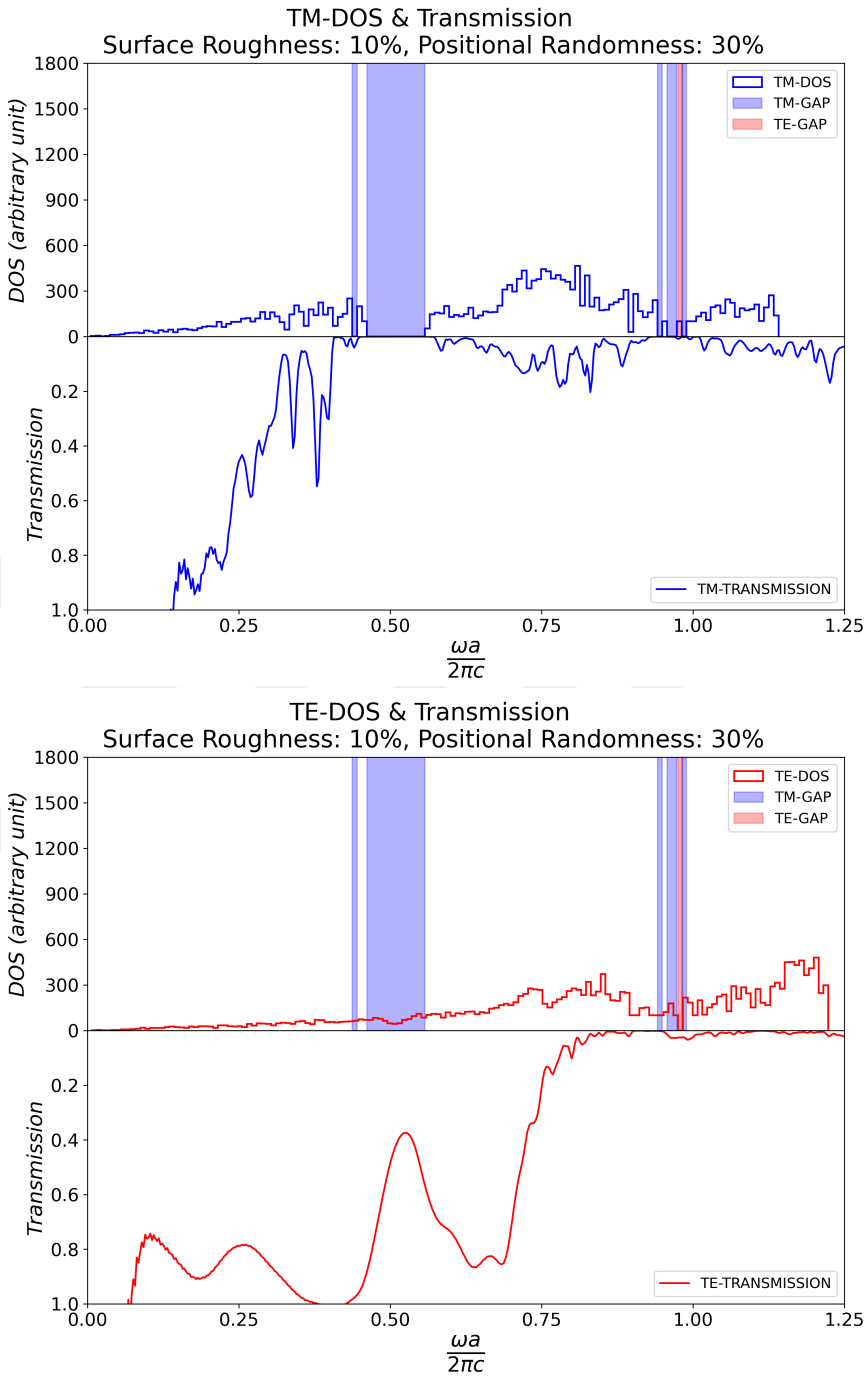

Figure 3.19. The DOS of the TM modes, TE modes over one hundered random $k-points$ and the transmission for the 10% surface roughness and 30% positional randomness.

CHAPTER 4

CONCLUSION

In this thesis, effect of structural variations on the optical properties of honeycomb photonic crystals is investigated. In the first case, surfaces of rods in the honeycomb lattice are randomly deformed in a systematic way in order to understand how deformation affects the density of states. We have used uniformly distributed random numbers in a range of various percentages of rod radius r. Next, we displaced rods with surface deformations, again by using uniformly distributed random numbers for the coordinates of rod centers. Centers are chosen on a disk whose radius changes by a fraction of the nearest neighbor distance a.

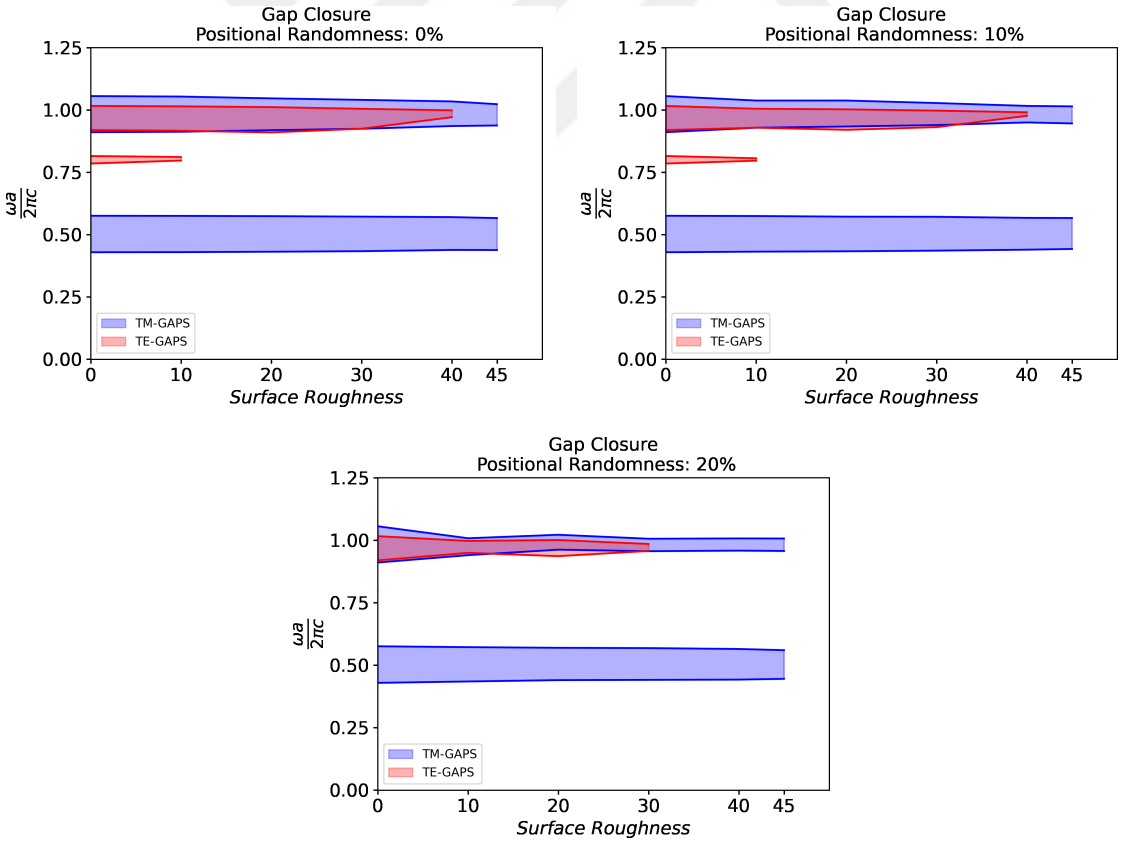

Figure 4.1. Gap closure plots for given surface roughness versus positional randomness.

According to the results, we are able to observe relatively small changes in DOS and transmission. Higher amount of random errors made significant changes in both. As percentage of errors increased, TM and TE gaps are narrowed and CPBG totally disappered at 45% of surface deformation. Similarly, when there was 10% of random shift with 45% of surface deformation CPBG was not observed. In addition, we encountered defect mode like modes when random shift took place. Especially, 10% and 20% random shift $40\%$and 30% surface deformation cases, if calculations will be repeated by using different random numbers CPBGs may vanish or vice versa. Transmission of deformed structures is also investigated in order to check if DOS calculations are consistent.

One need to beware of the fact that the calculations are done for single sample for each error percentages. There must be a statistical work in future.

REFERENCES

Asif, M. H., F. Elinder, and M. Willander (2011). Electrochemical biosensors based on zno nanostructures to measure intracellular metal ions and glucose. *J Anal Bioanal Tech. https://doi. org/10.4172/2155-9872. S7-003*.

Badreldin, T. and D. Khalil (2006). Monte carlo simulation of photonic band gap structures. In *2006 International Conference on MEMS, NANO, and Smart Systems*, pp. 52–57. IEEE.

Berenger, J.-P. (1994). A perfectly matched layer for the absorption of electromagnetic waves. *Journal of computational physics 114*(2), 185–200.

Chu, T., J. Chu, B. Gao, and B. He (2020). Modern evolution of paper-based analytical devices for wearable use: from disorder to order. *Analyst 145*(16), 5388–5399.

Cullen, D. K., Y. Xu, D. V. Reneer, K. D. Browne, J. W. Geddes, S. Yang, and D. H. Smith (2011). Color changing photonic crystals detect blast exposure. *Neuroimage 54*, S37–S44.

Economou, E. N. (2006). *Green's functions in quantum physics*, Volume 7. Springer Science & Business Media.

Feng, Z., X. Zhang, S. Feng, K. Ren, Z.-Y. Li, B. Cheng, and D. Zhang (2006). Effect of rotational randomness on focusing in a two-dimensional photonic-crystal flat lens. *Journal of Optics A: Pure and Applied Optics 9*(1), 101.

John, S. (1987). Strong localization of photons in certain disordered dielectric superlattices. *Physical review letters 58*(23), 2486.

Johnson, S. G. and J. D. Joannopoulos (2001). Block-iterative frequency-domain methods for maxwell s equations in a planewave basis. *Optics express 8*(3), 173–190.

Kim, J. K., J. H. Moon, T.-W. Lee, and J. H. Park (2012). Inverse opal tungsten trioxide films with mesoporous skeletons: synthesis and photoelectrochemical responses. *Chemical Communications 48*(98), 11939–11941.

Kong, X.-k., S.-b. Liu, H.-f. Zhang, and H.-l. Guan (2011). The effect of random variations of structure parameters on photonic band gaps of one-dimensional plasma photonic crystals. *Optics Communications 284*(12), 2915–2918.

Lagendijk, A. and B. A. Van Tiggelen (1996). Resonant multiple scattering of light. *Physics Reports 270*(3), 143–215.

Liu, H., Z. Li, R. Shen, Z. Li, Y. Yang, and Q. Yuan (2021). Point-of-care pathogen testing using photonic crystals and machine vision for diagnosis of urinary tract infections. *Nano Letters 21*(7), 2854–2860.

Meade, R. D., K. D. Brommer, A. M. Rappe, and J. Joannopoulos (1991). Photonic bound states in periodic dielectric materials. *Physical Review B 44*(24), 13772.

Meade, R. D., A. Rappe, K. Brommer, J. Joannopoulos, and O. Alerhand (1993). Accurate theoretical analysis of photonic band-gap materials. *Physical Review B 48*(11), 8434.

Meisels, R. and F. Kuchar (2007). Density-of-states and wave propagation in two-dimensional photonic crystals with positional disorder. *Journal of Optics A: Pure and Applied Optics 9*(9), S396.

Mouchet, S. R., S. Luke, L. T. McDonald, and P. Vukusic (2020). Optical costs and benefits of disorder in biological photonic crystals. *Faraday Discussions 223*, 9–48.

Oskooi, A. F., D. Roundy, M. Ibanescu, P. Bermel, J. D. Joannopoulos, and S. G. Johnson (2010). Meep: A flexible free-software package for electromagnetic simulations by the fdtd method. *Computer Physics Communications 181*(3), 687–702.

Sözüer, H. S., J. Haus, and R. Inguva (1992). Photonic bands: Convergence problems

with the plane-wave method. *Physical Review B 45*(24), 13962.

Sözüer, H. S. and K. Sevim (2005). Robustness of one-dimensional photonic band gaps under random variations of geometrical parameters. *Physical Review B 72*(19), 195101.

Taflove, A. and M. E. Brodwin (1975). Numerical solution of steady-state electromagnetic scattering problems using the time-dependent maxwell's equations. *IEEE transactions on microwave theory and techniques 23*(8), 623–630.

Taflove, A., A. Oskooi, and S. G. Johnson (2013). *Advances in FDTD computational electrodynamics: photonics and nanotechnology*. Artech house.

Vigneron, J. P. and P. Simonis (2012). Natural photonic crystals. *Physica B: Condensed Matter 407*(20), 4032–4036.

Yablonovitch, E. (1987). Inhibited spontaneous emission in solid-state physics and electronics. *Physical review letters 58*(20), 2059.

Yee, K. (1966). Numerical solution of initial boundary value problems involving maxwell's equations in isotropic media. *IEEE Transactions on antennas and propagation 14*(3), 302–307.

Yoo, Y. J., S.-Y. Heo, Y. J. Kim, J. H. Ko, Z. F. Mira, and Y. M. Song (2021). Functional photonic structures for external interaction with flexible/wearable devices. *Nano Research*, 1–15.

Zhang, C., J. Xu, and Y. Chen (2020). Preparation of monolayer photonic crystals from ag nanobulge-deposited sio2 particles as substrates for reproducible sers assay of trace thiol pesticide. *Nanomaterials 10*(6), 1205.